J. Fluid Mech. (1991), *vol.* 228, *pp.* 243–274
Printed in Great Britain

Normal shock-wave structure in two-phase vapour–droplet flows

By J. B. YOUNG AND A. GUHA
Whittle Laboratory, University of Cambridge, Madingley Road, Cambridge, CB3 0DY, UK

(Received 29 December 1989 and in revised form 14 September 1990)

A study of the structure of stationary, fully and partly dispersed, normal shock waves in steady vapour–droplet, two-phase flow is presented. Pure substances only are considered, but, unlike most previous work, the droplet population is allowed to be polydispersed. It is shown how the effects of thermal relaxation for such a mixture can be elegantly incorporated into the analysis.

Three types of fully dispersed wave are identified. Type I waves are dominated by thermal relaxation and an approximate analytical solution is presented which gives results in close agreement with accurate numerical solutions of the governing equations. The analysis predicts some unexpected behaviour of the thermodynamic variables and demonstrates the correct scaling parameters for such flows. An approximate analysis is also presented for Type II waves, dominated by both velocity and thermal relaxation. Type III waves, where all three relaxation processes are important, are of little practical significance and are only briefly discussed. Partly dispersed waves are also considered and the results of a numerical simulation of the relaxation zone are presented. A linearized solution of this problem is possible but, unlike other relaxing gas flows, does not give good agreement with the more exact numerical calculations.

The apparent discontinuity in the speed of sound in a vapour–droplet mixture as the wetness fraction tends to zero has been responsible for some confusion in the literature. This problem is reconsidered and it is shown that the transition from the two-phase equilibrium to the single-phase frozen shock wave speed is continuous.

1. Introduction

The thermo-fluid dynamics of the two-phase flow of a vapour–liquid mixture consisting of a large number of minute liquid droplets uniformly dispersed throughout a background vapour phase continuum is both scientifically interesting and of engineering importance. (Applications include condensing flows of moist air or combustion products, aerosol formation in mixing processes and wetness problems in steam turbines). Two-phase flows of this type respond well to mathematical modelling because the small size of the droplets (typically of radii less than 1 μm) and the magnitude of the surface tension forces ensure that droplet sphericity is maintained in most situations.

Most engineering applications of condensing flows involve complex geometrical boundaries (e.g. flow in turbine cascades) and it is not surprising that numerical methods of solution have, in the past, been stressed in preference to the analytical approach (Moheban & Young 1985; Bakhtar & Tochai 1980). Theoretical work has also focused more on the nucleation and initial growth of the droplet cloud rather than the equally important problem of the flow characteristics once the droplet

population is fully established. Thus, although numerical solutions of quite complicated two-dimensional nucleating flows can now be obtained, there are still fundamental areas where basic physical clarification is required. One such area is the structure of shock waves in non-nucleating vapour–droplet flows.

The interaction of the droplet cloud with the vapour continuum gives rise to a dispersive medium and the shock wave structure displays many of the characteristics to be found in other types of relaxing gas flows, such as those involving chemical dissociation or vibrational non-equilibrium. The vapour–droplet flow problem is more complicated, however, because three different relaxation processes can be identified (associated with thermal equilibrium of the droplets, interphase velocity slip and thermal equilibrium of the whole medium) and it is not immediately obvious exactly what role each particular process plays in the overall shock wave structure. Another difficulty is that the droplet cloud may not be monodispersed (i.e. droplets all of the same radius) but may exhibit an arbitrary level of polydispersity with a spectrum of droplet radii difficult to quantify.

In this paper we discuss the structure of stationary compressive normal shock waves in steady flows of vapour–droplet mixtures. For clarity, the analysis is restricted to pure substances (so that phase change is heat transfer rather than diffusion controlled), but the extension to include an inert carrier gas is also possible.

Although the propagation of small-amplitude harmonic waves in vapour–droplet mixtures has been studied extensively (Cole & Dobbins 1970; Petr 1973; Gumerov, Ivandaev & Nigmatulin 1988), the subject of shock waves in similar mixtures has not been addressed to any great extent. The general behaviour of condensing flows was examined by Marble (1969) who discussed the structure of partly dispersed shock waves (which consist of a near discontinuity dominated by viscosity and heat conduction, followed by a long relaxation zone), but did not mention the interesting possibility of fully dispersed waves which are stable in steady flow at velocities below the frozen speed of sound. Partly dispersed shock waves were also discussed by Konorski (1971) and Bakhtar & Yousif (1974), although these authors did not include any attempt at generalization. Petr (1979), by applying the formalism of relaxation gas dynamics, obtained a solution for a fully dispersed wave governed by just one relaxation process, but few details of his analysis are presented.

Shock waves in vapour–droplet flows have been studied experimentally in a number of different situations (although no measurements are available to provide a detailed picture of the structure of the waves). As examples, we cite the work of Barschdorff (1970) on periodically oscillating condensation zones in transonic nozzles and of Schnerr (1989) on the structure of two-dimensional moist air flows in channels and over aircraft wing sections. A recent article by Skillings (1989) shows some interesting unsteady shock wave behaviour in a transonic wet-steam turbine cascade. Measurements of shock propagation in moist air in a shock tube have also been performed by Goossens *et al.* (1989). Experiments such as these have led us to undertake the theoretical study reported below.

The present work examines the structure of fully and partly dispersed normal shock waves and clarifies the roles played by the various relaxation processes. Some progress is also made in including the effects of droplet polydispersity. In order to elucidate the underlying physics, a simplified analytical approach is used wherever possible. The results of numerical calculations are also presented so that the reader may readily appreciate the errors incurred by the approximations of the analytical methods. In many cases, surprisingly accurate estimates of, for example, shock wave velocity profiles can be obtained from quite simple calculations.

2. Conservation equations

We consider the one-dimensional steady flow of a wet vapour in a duct of constant cross-sectional area. The vapour is the continuous phase and has pressure p, temperature T_g, density ρ_g, specific enthalpy h_g and velocity V_g all of which are functions only of x, the distance in the flow direction measured from an arbitrary datum. The droplet population may be polydispersed and the continuous spectrum of droplet sizes is discretized into an arbitrary number of droplet groups. Group i consists of n_i droplets per unit mass of mixture, all of radius r_i, liquid density ρ_f and mass $m_i = \frac{4}{3}\pi r_i^3 \rho_f$. The contribution y_i of droplet group i to the total wetness fraction y is given by $y_i = n_i m_i$ and

$$y = \sum y_i = \sum n_i m_i, \tag{1}$$

where the summation sign signifies summation over all droplet groups. All droplets in a particular group are assumed to have the same velocity V_i and temperature T_i, the latter being assumed uniform throughout a droplet.

The analysis is valid for low wetness fractions such that the volume occupied by the liquid phase is negligible. Also neglected is the partial pressure of the droplet cloud. In calculating h_i, the specific enthalpy of a droplet in group i, the contribution from the surface energy is not included. It is also assumed that the change in vapour pressure due to droplet surface curvature is small.

The droplet cloud is assumed to be uniformly distributed throughout the vapour and of sufficient number density that the interaction with the vapour can be described by a continuous variation. We therefore adopt what is commonly called the 'two-fluid' model and view the droplets as providing sources or sinks of mass, momentum and energy for the vapour, each source term varying continuously in the x-direction. Coagulation of droplets is neglected and individual droplet radii change solely by pure evaporation or condensation. In passing through a shock wave, each droplet is assumed to retain its individual identity. Indeed, for the types of flow considered here, the Weber-number criterion for stability against fragmentation is well satisfied even for very strong shock wave deceleration.

For clarity, the analysis is presented for the flow of a pure substance only (i.e. the vapour phase and the liquid droplets are of the same chemically pure species), but the extension to include an inert carrier gas is also possible.

The assumptions detailed in the previous paragraphs may appear restrictive at first glance but in practice this is not the case and the analysis applies to most wet vapour flows formed initially by homogeneous nucleation and having wetness fractions less than about 0.2. As an example, consider the case of a monodispersed population of water droplets in steam at a pressure of 0.5 bar and a corresponding saturation temperature T_s of 81.3 °C. Depending on the rate of expansion during the nucleation process, the final, established, droplet radius would be expected to lie in the range 0.05–2.0 μm. For a wetness fraction of 0.2, this corresponds to a number concentration varying from 1.5×10^{11} cm^{-3} to 2.4×10^6 cm^{-3}. The average distance between droplets is about 23 droplet diameters and the volume fraction occupied by the liquid phase is only 8×10^{-5}. In passing through a strong shock wave generating an interphase slip velocity ΔV of 200 m/s, say, the range of Weber number ($2r\rho_g \Delta V^2/\sigma$, where σ is the liquid surface tension) corresponding to the given range of droplet radii is 0.02–0.7, which is well within the stability limit.

The neglect of the surface energy terms implies that the droplets are well established after the nucleation process, but again this is not a serious restriction.

The Kelvin–Helmholtz equation giving the vapour subcooling ($\Delta T = T_s - T_g$) for equilibrium of a droplet of radius r is

$$\Delta T = \frac{2\sigma T_s}{\rho_f h_{fg} r}, \tag{2}$$

where ρ_f is the liquid density and h_{fg} is the specific enthalpy of evaporation. For the condition specified above, we find that, for $r = 0.05$ μm, $\Delta T = 0.43$ °C and for $r = 2.0$ μm, $\Delta T = 0.01$ °C.

Adopting the assumptions discussed above, it is straightforward to derive the basic conservation equations for the flow. Firstly, the conservation of droplets is represented by

$$\frac{\mathrm{d}}{\mathrm{d}x}\left(\frac{n_i \rho_g V_i}{1-y}\right) = 0, \tag{3}$$

there being one equation for each droplet group.

The mass continuity, momentum and energy equations for the two-phase mixture (assuming the flow to be inviscid and thermally non-conducting) are

$$\frac{\mathrm{d}}{\mathrm{d}x}\left(\rho_g V_g + \sum \frac{y_i \rho_g V_i}{1-y}\right) = 0, \tag{4}$$

$$\frac{\mathrm{d}}{\mathrm{d}x}\left(p + \rho_g V_g^2 + \sum \frac{y_i \rho_g V_i^2}{1-y}\right) = 0, \tag{5}$$

$$\frac{\mathrm{d}}{\mathrm{d}x}\left[\rho_g V_g (h_g + \tfrac{1}{2}V_g^2) + \sum \frac{y_i \rho_g V_i}{1-y}(h_i + \tfrac{1}{2}V_i^2)\right] = 0. \tag{6}$$

We assume that the vapour phase behaves as a perfect gas with constant isobaric specific heat capacity c_p. Thus,

$$\frac{\mathrm{d}}{\mathrm{d}x}\left(\frac{p}{\rho_g R T_g}\right) = 0, \tag{7}$$

$$\frac{\mathrm{d}h_g}{\mathrm{d}x} = c_p \frac{\mathrm{d}T_g}{\mathrm{d}x}, \tag{8}$$

where R is the specific gas constant of the vapour. The perfect gas approximation is not crucial to the analysis. More realistic equations of state can be introduced if desired but these tend to complicate the algebraic development and do not provide any further physical insight.

In later sections, we shall specify the thermal equilibrium state by the saturation temperature rather than the pressure. The two are related by the Clausius–Clapeyron equation. Neglecting the specific volume of the liquid and introducing the perfect gas equation for the vapour phase, we have

$$\frac{1}{p}\frac{\mathrm{d}p}{\mathrm{d}x} = \frac{h_{fg}}{R T_s}\frac{1}{T_s}\frac{\mathrm{d}T_s}{\mathrm{d}x}. \tag{9}$$

3. Relaxation processes

The set of equations in the previous section is incomplete and must be supplemented by three equations for each droplet group, representing the interphase transport of mass, momentum and energy. If the velocity slip between droplets and

vapour is small, the mass and energy transfer equations can be decoupled from the momentum transfer equation which, for an i-group droplet, can then be written

$$m_i V_i \frac{\mathrm{d}V_i}{\mathrm{d}x} = D_i, \tag{10}$$

where D_i is the drag force exerted by the vapour on an i-group droplet.

The mass and energy transfer equations are strongly coupled and take the form (Young 1982)

$$V_i \frac{\mathrm{d}m_i}{\mathrm{d}x} = -M_i, \tag{11}$$

$$m_i V_i \frac{\mathrm{d}h_i}{\mathrm{d}x} = -(h_\mathrm{g} - h_i) M_i - Q_i, \tag{12}$$

where M_i is the mass transfer rate and Q_i is the heat transfer rate from an i-group droplet. The term $(h_\mathrm{g} - h_i)$ can normally be replaced by the specific enthalpy of evaporation h_{fg} with negligible error.

Definitive expressions do not exist for D_i, M_i and Q_i. Problems arise because the flow in the vicinity of very small droplets does not satisfy continuum requirements. The droplet Knudsen number ($Kn_i = \delta/2r_i$, where δ is the mean free path of a vapour molecule) can span the range from the continuum ($Kn_i \ll 1$) to the free-molecule regime ($Kn_i \gg 1$) and it is necessary to postulate equations valid over the whole of this range. This paper is not concerned with the finer points of droplet growth theory and we shall employ equations which are reasonably well established and of the shape most commonly used by workers in the field.

For the small droplets considered here, the only contribution to D_i of any significance is the steady-state drag force. Following Gyarmathy (1964), we take

$$D_i = \frac{6\pi r_i \mu}{\phi(Re_i) + 4.5 Kn_i} (V_\mathrm{g} - V_i), \tag{13}$$

where μ is the dynamic viscosity of the vapour and $\phi(Re_i)$ is an empirical correction based on slip Reynolds number ($Re_i = 2\rho_\mathrm{g} r_i |V_\mathrm{g} - V_i|/\mu$) given by

$$\phi(Re_i) = [1 + 0.15 Re_i^{0.687}]^{-1}. \tag{14}$$

In calculating the vapour molecular mean free path for evaluating Kn_i, we use the simple kinetic theory expression

$$\delta = \frac{\mu}{p} (\tfrac{1}{2}\pi R T_\mathrm{g})^{\frac{1}{2}}. \tag{15}$$

For small slip Reynolds numbers and continuum flow ($Re_i \ll 1$, $Kn_i \ll 1$) equation (13) reduces to the Stokes drag formula for a sphere. For free-molecule flow ($Kn_i \gg 1$) an expression derivable from kinetic theory is obtained. The denominator of (13) provides a simple interpolation formula (Cunningham 1910) for intermediate Knudsen numbers.

A similar approach is used to specify the heat transfer rate Q_i. Again, following Gyarmathy (1976), we take,

$$Q_i = \frac{4\pi r_i \lambda}{1 + 4.5 Kn_i / Pr} (T_i - T_\mathrm{g}), \tag{16}$$

where λ is the thermal conductivity and $Pr = c_p \mu/\lambda$ is the Prandtl number of the vapour. The factor 4.5 appears rather than the more usual 3.8 because of our

definition of the mean free path. For small Kn_i, equation (16) reduces to the continuum expression for steady-state conduction heat transfer from a sphere. For large Kn_i the kinetic theory (free molecule) result is regained.

When a droplet is condensing or evaporating, the radial mass motion of the vapour may affect the form of D_i and Q_i. This is a difficult problem to address but, in all cases considered here, the vapour velocity induced by the phase change is very small and neglect of the effect appears justifiable.

The mass transfer rate M_i is more difficult to specify and has been the subject of extensive debate in recent years (Labuntsov & Kryukov 1979). For many droplet growth calculations, however, the form is not critical and following Young (1982) we use

$$M_i = 4\pi r_i^2 \frac{2q}{2-q}\left[\frac{p_s(T_i)}{(2\pi R T_i)^{\frac{1}{2}}} - \frac{p}{(2\pi R T')^{\frac{1}{2}}}\right], \tag{17}$$

where

$$\frac{T'-T_g}{T_i-T_g} = \frac{1}{1+4.5Kn_i/Pr}, \tag{18}$$

and $p_s(T_i)$ is the saturation pressure at the droplet temperature T_i. In keeping with earlier assumptions, changes of vapour pressure with droplet surface curvature have been neglected.

Equations (17) and (18) are obtained from a simple kinetic theory model which assumes free-molecule behaviour in a region close to the droplet surface and continuum behaviour in an outer region far from the droplet. T' represents the temperature at the interface of the two regions which is assumed to occur at a distance of about one mean free path from the droplet surface. Expression (18) is a slightly simplified form of that presented in Young (1982), chosen to be compatible with equation (16).

The condensation coefficient q in (17) is a parameter lying between 0 and 1 representing the fraction of molecules incident on the droplet which condenses (as opposed to being reflected). The magnitude of q has been discussed for over half a century and the argument is still not resolved (Mozurkewich 1986). In keeping with modern thought we shall adopt a value of $q = 1$ for numerical computation.

The expressions for D_i, Q_i and M_i are too cumbersome to utilize in any analytical procedure and it is advantageous to introduce three relaxation times for each droplet group, characterizing the response of the two-phase system to departures from equilibrium. To a certain extent, the definitions of the relaxation times are arbitrary, but it is profitable to exploit the physics of the problem and choose relaxation processes which are almost independent.

Relaxation associated with velocity slip is the most straightforward, although not the most important, process. We define the slip velocity $\Delta V_i = (V_g - V_i)$ as the non-equilibrium variable, and (10) combined with (13) can then be written

$$\frac{\mathrm{d}(\Delta V_i)}{\mathrm{d}x} + \frac{\Delta V_i}{V_i \tau_{Ii}} = \frac{\mathrm{d}V_g}{\mathrm{d}x}. \tag{19}$$

the local i-group velocity (or inertial) relaxation time τ_{Ii} is defined by

$$\tau_{Ii} = \frac{2r_i^2 \rho_f}{9\mu}[\phi(Re_i) + 4.5Kn_i]. \tag{20}$$

Each droplet group is associated with a particular relaxation time which varies from point to point in the flow field. This variation can easily be accommodated in a numerical integration procedure but, in the analytical development, we shall adopt

suitable average values and assume the relaxation times to remain constant. No physical principles are obscured by this approximation and the accuracy of the assumption (which is normally very good, especially for fully dispersed waves) can be judged by comparison with the numerical results.

The reversion to thermal equilibrium following a disturbance usually takes place in two, almost independent, stages. Suppose the medium to be perturbed from equilibrium so that neither the vapour temperature T_g nor the droplet temperatures T_i equal the saturation temperature T_s. In the first (normally extremely rapid) stage of relaxation, the droplet temperatures approach exponentially steady-state values $T_{i\infty}$ which are usually very close to the saturation temperature. In this first relaxation period, the change in droplet temperature is caused by the condensation (or evaporation) of a comparatively small mass which supplies (or removes) the required energy. If the droplets are small, their radii hardly change and negligible heat is transferred between the phases. In the second (much longer) stage of relaxation, the vapour temperature rises (or falls) to the saturation value due to the interphase heat transfer as the droplets grow (or evaporate).

We investigate below the conditions under which the thermal relaxation process naturally divides into two periods of quite different timescale. However, whether or not these conditions are fulfilled, it is shown in Appendix A that (12) can always be written in the form

$$\frac{\mathrm{d}T_i}{\mathrm{d}x}+\frac{T_i-T_{i\infty}}{V_i\tau_{\mathrm{D}i}}=0, \tag{21}$$

where $T_{i\infty}$ is the steady-state droplet temperature defined by equation (A 2) in Appendix A and

$$\tau_{\mathrm{D}i}=\frac{1}{1-A}\frac{2-q}{2q}\left(\frac{RT_s}{h_{fg}}\right)^2\frac{r_i\rho_f c_f}{3R}\frac{(2\pi RT_s)^{\frac{1}{2}}}{p}, \tag{22}$$

c_f being the specific heat capacity of the liquid and the parameter A being defined by equation (A 3) in Appendix A. In the Appendix, it is shown that $A \ll 1$ for all common substances unless the condensation coefficient q is also very small.

The form of (21) shows clearly that $\tau_{\mathrm{D}i}$ can be interpreted physically as the droplet temperature relaxation time for group-i droplets. The conjugate non-equilibrium variable is defined as $\Delta T_i = (T_{i\infty}-T_i)$ although, in most practical cases $T_{i\infty} \approx T_s$ and $\Delta T_i \approx (T_s-T_i)$. After a small disturbance from equilibrium, the steady-state droplet temperature $T_{i\infty}$ is approached exponentially with time constant $\tau_{\mathrm{D}i}$. In passing, we note that, in his analysis, Marble (1969) identified correctly the physical processes resulting in droplet temperature relaxation but his expression for the relaxation time itself was in error. This was because he did not define the relaxation time via an archetypal equation like (21). The expression given by Jackson & Davidson (1983) is also incorrect for the same reason.

Using (21) and the definition (22) for $\tau_{\mathrm{D}i}$, (11) and (12) can be combined to give an expression for the growth rate of group-i droplets, which is conveniently expressed in the form

$$(h_g-h_i)\,n_i\frac{\mathrm{d}m_i}{\mathrm{d}x}=\frac{(1-y)\,c_p(T_i-T_g)}{V_i\tau_{\mathrm{T}i}}+\frac{y_i c_f\Delta T_i}{V_i\tau_{\mathrm{D}i}}, \tag{23}$$

where $\tau_{\mathrm{T}i}$ is defined by

$$\tau_{\mathrm{T}i}=\frac{(1-y)\,c_p r_i^2\rho_f}{3\lambda y_i}\left(1+\frac{4.5Kn_i}{Pr}\right). \tag{24}$$

Although $\tau_{\mathrm{T}i}$ has the units of time, it does not, by itself represent the thermal relaxation time of the whole medium unless the droplet population is mono-

dispersed. The vapour temperature responds simultaneously to heat transfer from all size classes of droplets and all droplets are instrumental in raising or lowering the temperature to the saturation value. This is quite unlike velocity and droplet temperature relaxation where it is possible for some droplets to be in equilibrium with the vapour while others are still relaxing.

To identify the vapour thermal relaxation time, it is necessary to consider the integrated effect of the droplet cloud as a whole. The analysis is outlined in Appendix A where it is shown that the vapour thermal relaxation time τ_T is given by

$$\frac{1}{\tau_T} = \sum \frac{1}{\tau_{Ti}}, \tag{25}$$

the summation extending over all droplet groups. In passing, we note that the vapour thermal relaxation time defined by Marble (1969) does not have the correct physical significance because he failed to include the integrated effect of all the droplets and did not manipulate the equations into the archetypal relaxation form when making his definition.

The equations of Appendix A and the definition (25) of τ_T show how the effects of a polydispersion may be introduced without direct specification of the form of the droplet size distribution. Thus, assuming the droplet cloud to be well established, different distributions with the same value of τ_T affect the gross flow behaviour in identical ways. Unfortunately, however, this elegant simplification is restricted in application to the vapour thermal relaxation process and cannot be extended to the droplet temperature and velocity relaxation processes. Hence, for a droplet spectrum discretized into N droplet groups, we are still faced with a multi-phase flow exhibiting $2N+1$ different relaxation times. Luckily, this apparently intractable problem can be naturally simplified in other ways.

One obvious approach is suggested by the fact that, for the small droplets considered here, the three relaxation times are of quite different magnitudes. Droplet temperature relaxation is much faster than velocity relaxation, which is itself about one order of magnitude faster than vapour thermal relaxation. Indeed, considering for the moment a monodispersed droplet population, we find from the ratio of (20) and (24) for $Pr = 1$ and $Re \to 0$,

$$\frac{\tau_I}{\tau_T} = \frac{2y}{3(1-y)}, \tag{26}$$

a ratio which is always less than 0.17 by the terms of the analysis ($y < 0.2$). The ratio of (22) and (24) gives

$$\frac{\tau_D}{\tau_T} = \frac{1}{1-A}\frac{2-q}{2q}\frac{y}{1-y}\frac{c_f}{R}\left(\frac{RT_s}{h_{fg}}\right)^2 \frac{Kn/Pr}{1+4.5Kn/Pr}. \tag{27}$$

This shows that, for most common substances, the droplet temperature relaxation time τ_D is several orders of magnitude less than the vapour thermal relaxation time τ_T, the exception to this general rule being in the unlikely event that $q \ll 1$.

In the analysis that follows, we exploit the disparity in relaxation times and henceforth assume

$$\tau_D \ll \tau_I \ll \tau_T. \tag{28}$$

As a practical illustration, figure 1 shows curves of τ_D, τ_I and τ_T as functions of droplet radius, plotted for a monodispersed population of water droplets in steam at 0.5 bar pressure and wetness fraction 0.1. In this particular case it is evident that the inequalities (28) are well satisfied.

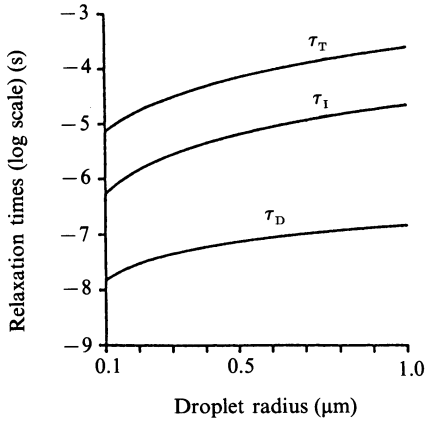

FIGURE 1. Droplet temperature, velocity slip and vapour thermal relaxation times for monodispersed water droplets in pure steam; $p = 0.5$ bar, $y = 0.1$.

To summarize the results of this section, the conservation equations (3)–(6) are supplemented by three interphase transfer equations (19), (21) and (23) for each droplet group. For future reference these are now collected together and written in a slightly more convenient form as

$$\frac{\mathrm{d}V_i}{\mathrm{d}x} = \frac{\Delta V_i}{V_i \tau_{\mathrm{I}i}}, \tag{29}$$

$$\frac{\mathrm{d}T_i}{\mathrm{d}x} = \frac{\Delta T_i}{V_i \tau_{\mathrm{D}i}}, \tag{30}$$

$$(h_{\mathrm{g}} - h_i)\, n_i \frac{\mathrm{d}m_i}{\mathrm{d}x} = \frac{(1-y)\, c_p \Delta T}{V_i \tau_{\mathrm{T}i}} + \frac{y_i c_{\mathrm{f}} \Delta T_i}{V_i \tau_{\mathrm{D}i}}, \tag{31}$$

where $\Delta V_i = (V_{\mathrm{g}} - V_i)$, $\Delta T_i = (T_{\mathrm{s}} - T_i)$, $\Delta T = (T_{\mathrm{s}} - T_{\mathrm{g}})$ and $\tau_{\mathrm{I}i}$, $\tau_{\mathrm{D}i}$ and $\tau_{\mathrm{T}i}$ are given by (20), (22) and (24) respectively. (For ease of interpretation in later sections, slight simplifications have been made to (21) and (23). It is shown in Appendix A that the steady-state droplet temperature $T_{i\infty}$ varies only slightly from the saturation temperature T_{s}. In (30) and (31) we have therefore made the assumption $T_{i\infty} = T_{\mathrm{s}}$ and in (31) $\tau_{\mathrm{D}i} \ll \tau_{\mathrm{T}i}$.)

4. Working forms of the basic equations

Straightforward algebraic manipulation of (3)–(8) leads to the following forms of the three conservation equations:

$$\frac{\mathrm{D}p}{p} - \frac{\mathrm{D}T_{\mathrm{g}}}{T_{\mathrm{g}}} + \frac{\mathrm{D}V_{\mathrm{g}}}{V_{\mathrm{g}}} + \frac{1}{V_{\mathrm{g}}} \sum \frac{n_i V_i \mathrm{D}m_i}{1-y} = 0, \tag{32}$$

$$\frac{\mathrm{D}p}{p} + \frac{V_{\mathrm{g}}^2}{RT_{\mathrm{g}}} \left\{ \frac{\mathrm{D}V_{\mathrm{g}}}{V_{\mathrm{g}}} + \frac{1}{V_{\mathrm{g}}} \sum \frac{y_i}{1-y} \frac{V_i}{V_{\mathrm{g}}} \mathrm{D}V_i + \frac{1}{V_{\mathrm{g}}} \sum \frac{V_i - V_{\mathrm{g}}}{V_{\mathrm{g}}} \frac{n_i V_i \mathrm{D}m_i}{(1-y)} \right\} = 0, \tag{33}$$

$$\frac{\mathrm{D}T_{\mathrm{g}}}{T_{\mathrm{g}}} + \sum \frac{y_i}{1-y} \frac{c_{\mathrm{f}}}{c_p} \frac{V_i}{V_{\mathrm{g}}} \frac{\mathrm{D}T_i}{T_{\mathrm{g}}} + \frac{V_{\mathrm{g}}^2}{c_p T_{\mathrm{g}}} \left\{ \frac{\mathrm{D}V_{\mathrm{g}}}{V_{\mathrm{g}}} + \sum \frac{y_i}{1-y} \left(\frac{V_i}{V_{\mathrm{g}}} \right)^2 \frac{\mathrm{D}V_i}{V_{\mathrm{g}}} \right\}$$
$$- \sum \frac{(h_{\mathrm{g}} - h_i)}{c_p T_{\mathrm{g}}} \frac{n_i V_i \mathrm{D}m_i}{V_{\mathrm{g}}(1-y)} - \sum \frac{(V_{\mathrm{g}}^2 - V_i^2)}{2c_p T_{\mathrm{g}}} \frac{n_i V_i \mathrm{D}m_i}{V_{\mathrm{g}}(1-y)} = 0. \tag{34}$$

The convenient shorthand $\mathrm{D} = \mathrm{d}/\mathrm{d}x$ has been introduced and it will be noted that the variable ρ_g has been eliminated to leave the three dependent variables p, T_g, V_g characterizing the vapour state.

The results of the analysis will show that the quantities $(\Delta T/T_g)$, $(\Delta V_i/V_g)$ and $(\Delta T_i/T_s)$ are all much less than unity. When (31) is substituted into (33) and (34), the final term in each of these equations contains the products $(\Delta V_i/V_g)(\Delta T/T_g)$ and $(\Delta V_i/V_g)(\Delta T_i/T_s)$ which are of second order in small quantities. Although it is possible to retain these terms in the analysis, we gain neither accuracy nor insight by their inclusion and they are henceforth neglected. The basic working equations therefore become

$$\frac{\mathrm{D}p}{p} - \frac{\mathrm{D}T_g}{T_g} + \frac{\mathrm{D}V_g}{V_g} + \sum \frac{V_i}{V_g} \frac{n_i \mathrm{D}m_i}{1-y} = 0, \tag{35}$$

$$\frac{\mathrm{D}p}{p} + \frac{V_g^2}{RT_g} \left\{ \frac{\mathrm{D}V_g}{V_g} + \sum \frac{y_i}{1-y} \frac{V_i}{V_g} \frac{\mathrm{D}V_i}{V_g} \right\} = 0, \tag{36}$$

$$\frac{\mathrm{D}T_g}{T_g} + \frac{c_f}{c_p} \sum \frac{y_i}{1-y} \frac{V_i}{V_g} \frac{\mathrm{D}T_i}{T_g} + \frac{V_g^2}{c_p T_g} \left\{ \frac{\mathrm{D}V_g}{V_g} + \sum \frac{y_i}{1-y} \left(\frac{V_i}{V_g} \right)^2 \frac{\mathrm{D}V_i}{V_g} \right\} - \sum \frac{h_g - h_i}{c_p T_g} \frac{V_i}{V_g} \frac{n_i \mathrm{D}m_i}{1-y} = 0. \tag{37}$$

5. Speeds of sound

We now introduce four reference velocities corresponding to the speed of sound in two-phase flow under different thermal and mechanical constraints. The full frozen and full equilibrium sound speeds are well known (Petr 1973). The former (denoted here by a_f) corresponds to the speed of an harmonic acoustic wave of such high frequency that the response of the droplets is negligible (i.e. zero mass, momentum and energy transfer). The latter (denoted here by a_{e3}) corresponds to the speed of an harmonic acoustic wave of such low frequency that liquid–vapour equilibrium is maintained at all times. The two intermediate speeds correspond to (*a*) the case of equilibrium droplet temperature relaxation but frozen momentum and heat transfer (a_{e1}) and, (*b*) the case of equilibrium droplet temperature and velocity relaxation but frozen heat transfer (a_{e2}).

The derivation of the sound speeds is quite straightforward and parallels the simple analysis, to be found in most elementary textbooks, for the speed of sound in single-phase flow. Figure 2 shows a stationary plane wave in a one-dimensional duct and the conservation equations (35)–(37) are applied across the wave and solved to give the vapour flow velocity relative to the wave under the specific constraints of interest. As an example, we describe the procedure to compute the sound speed a_{e2} corresponding to equilibrium droplet temperature and velocity, but frozen heat transfer.

Equilibrium velocity slip throughout the wave implies immediate velocity relaxation, so that $\mathrm{d}V_i/\mathrm{d}x = \mathrm{d}V_g/\mathrm{d}x$ in (35)–(37). (In (29) we allow ΔV_i and τ_{Ii} to tend to zero simultaneously, $\mathrm{d}V_i/\mathrm{d}x$ remaining finite.) Similarly, equilibrium droplet temperature implies $\mathrm{d}T_i/\mathrm{d}x = \mathrm{d}T_s/\mathrm{d}x$ in (35)–(37) and, in (30), ΔT_i and τ_{Di} tend simultaneously to zero. Finally, zero heat transfer implies $\tau_{Ti} \to \infty$ and (31) with (30) becomes

$$\frac{\mathrm{D}m_i}{m_i} = \frac{c_f T_s}{h_{fg}} \frac{\mathrm{D}T_s}{T_s}. \tag{38}$$

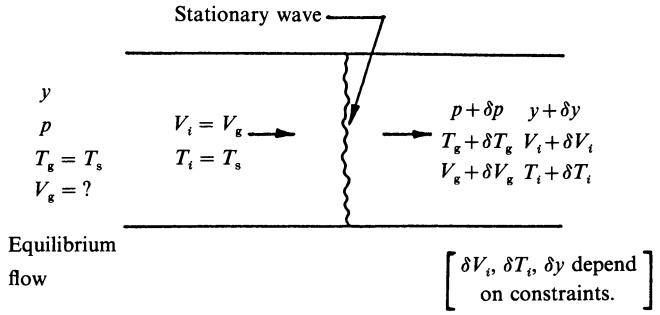

FIGURE 2. Flow configuration for calculation of the various sound speeds.

When this procedure is applied in turn for each sound speed, we obtain the following four expressions:

$$a_f^2 = \gamma R T_g, \tag{39}$$

$$a_{e1}^2 = \frac{\gamma R T_g}{1+(y/(1-y))\,(\gamma c_f/R)\,(RT_s/h_{fg})^2}, \tag{40}$$

$$a_{e2}^2 = \frac{(1-y)\,\gamma R T_g}{1+(y/(1-y))\,(\gamma c_f/R)\,(RT_s/h_{fg})^2}, \tag{41}$$

$$a_{e3}^2 = \frac{(1-y)\,\gamma R T_g}{\gamma[1-(RT_s/h_{fg})\,(2-cT_s/h_{fg})]}, \tag{42}$$

where $c = c_p + yc_f/(1-y)$. The ratio of specific heat capacities for the vapour phase is denoted by γ.

For small wetness fractions ($y \to 0$), it should be noted that a_{e1} and a_{e2} both tend to a_f, but

$$a_{e3}^2 \to \frac{\gamma R T_g}{1+(\gamma-1)\,(1-c_p T_s/h_{fg})^2}. \tag{43}$$

The fact that there appears to be a discontinuity in sound speed on crossing the saturation line has been a source of confusion in the literature. We reconsider this problem later in the paper.

The relationship of the four sound speeds to each other is of great importance. As a typical example, for steam at 1 bar pressure and wetness fraction 0.1, we find

$$a_f : a_{e1} : a_{e2} : a_{e3} \equiv 1 : 0.997 : 0.945 : 0.878.$$

6. Qualitative aspects of shock structure

We now consider the structure of stationary, finite-amplitude waves in one-dimensional, steady flow. Far upstream of the wave the flow is assumed to be in equilibrium with a specified pressure, wetness fraction and droplet size distribution. Far downstream of the wave a new equilibrium condition is re-established. The far upstream condition is denoted by subscript 0.

By applying the conservation equations between the upstream and downstream equilibrium states, it follows that the upstream flow velocity V_{g0} must exceed the full equilibrium speed of sound a_{e30} in order for a solution to exist other than the trivial case when all flow properties remain constant. It is also found, as with other types

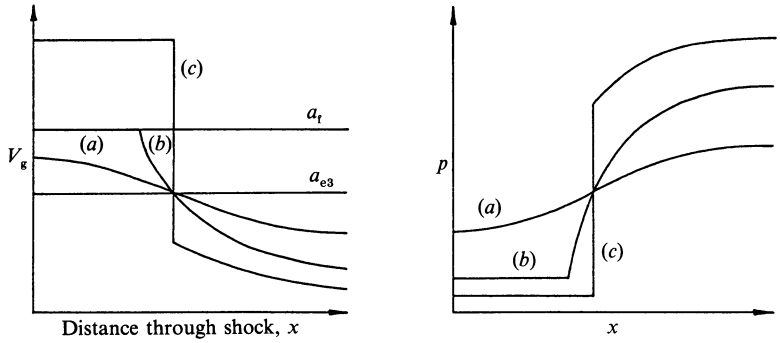

FIGURE 3. Schematic diagram of the structure of fully and partly dispersed shock waves. (*a*) Fully dispersed wave, (*b*) limiting case of fully dispersed wave (*c*) partly dispersed wave.

of relaxing gas flow (Vincenti & Kruger 1965), that a continuous transition of fluid properties can occur between the upstream and downstream equilibrium states, providing the upstream flow velocity is less than the fully frozen speed of sound a_{f0}. For this range of upstream flow velocities ($a_{e30} < V_{g0} < a_{f0}$), the steepening effect of the nonlinear terms in the equations of motion is just balanced by the dispersive effect of the relaxation processes. Such waves are described as fully dispersed.

For upstream flow velocities greater than a_{f0}, the conservation equations do not admit a continuous solution and a very steep-fronted shock wave forms in which the flow is dominated by the effects of viscosity and thermal conductivity. This part of the wave is normally modelled by a discontinuity in the flow properties and downstream of the discontinuity there is a continuous relaxation zone where the flow relaxes to its final equilibrium state. Such waves are described as partly dispersed.

Figure 3 shows a qualitative sketch of the pressure and vapour phase velocity distributions through the different types of wave. The temperature distribution is a little more complicated and we shall return to this later.

From a qualitative point of view, we have described nothing other than the well-known types of stationary wave to be found in all relaxing gas flows. However, one important result of our work shows that fully dispersed waves in vapour–droplet flows can be subdivided into three further categories depending on the upstream vapour phase velocity. We thus define

Type I waves corresponding to $a_{e30} < V_{g0} < a_{e20}$,

Type II waves corresponding to $a_{e20} < V_{g0} < a_{e10}$,

Type III waves corresponding to $a_{e10} < V_{g0} < a_{f0}$.

As we shall demonstrate, Type I waves are dominated by vapour thermal relaxation, Type II waves by both velocity and vapour thermal relaxation and Type III waves by all three relaxation processes. The remainder of this paper is devoted to a quantitative description of the various types of shock wave structure.

7. Fully dispersed waves of Type I

7.1. *The velocity profile of the wave*

Type I waves have upstream values of velocity which satisfy $a_{e30} < V_{g0} < a_{e20}$. For such waves, we shall show *a posteriori* that an excellent approximation is to assume that the droplet temperatures T_i and velocities V_i instantaneously accommodate to

their equilibrium values at all points within the wave. Formally, therefore, we allow τ_{Di} and τ_{Ii} to tend to zero, the ratios $\Delta T_i/\tau_{Di}$ and $\Delta V_i/\tau_{Ii}$ remaining finite such that

$$\frac{\Delta T_i}{\tau_{Di}} \to V_g \frac{dT_s}{dx}; \quad \frac{\Delta V_i}{\tau_{Ii}} \to V_g \frac{dV_g}{dx}. \tag{44a,b}$$

Substituting these approximations and (31) into the conservation equations (35)–(37), we obtain the set of governing equations for a Type I wave

$$\frac{Dp}{p} - \frac{DT_g}{T_g} + \frac{DV_g}{V_g} + \frac{y}{1-y}\frac{c_f T_s}{h_{fg}}\frac{DT_s}{T_s} + \frac{c_p T_g}{h_{fg}}\frac{\Delta T}{V_g \tau_T T_g} = 0, \tag{45}$$

$$\frac{Dp}{p} + \frac{V_g^2}{(1-y)RT_g}\frac{DV_g}{V_g} = 0, \tag{46}$$

$$\frac{DT_g}{T_g} + \frac{V_g^2}{(1-y)c_p T_g}\frac{DV_g}{V_g} - \frac{\Delta T}{V_g \tau_T T_g} = 0. \tag{47}$$

Starting from (45), we use (9) to eliminate DT_s/T_s and (46) to eliminate Dp/p. The result is

$$\frac{DV_g}{V_g}\left\{1 - \frac{V_g^2}{(1-y)RT_g}\left[1 + \frac{y}{1-y}\frac{c_f}{R}\left(\frac{RT_s}{h_{fg}}\right)^2 - \frac{T_s}{T_g}\frac{RT_s}{h_{fg}}\right]\right\} + \frac{D(\Delta T)}{T_g} + \frac{c_p T_g}{h_{fg}}\frac{\Delta T}{V_g \tau_T T_g} = 0. \tag{48}$$

Starting from (47) and again using (9) and (46), we obtain

$$\frac{DV_g}{V_g}\left[\frac{V_g^2}{(1-y)RT_g}\right]\left[\frac{T_s}{T_g}\frac{RT_s}{h_{fg}} - \frac{\gamma-1}{\gamma}\right] + \frac{D(\Delta T)}{T_g} + \frac{\Delta T}{V_g \tau_T T_g} = 0. \tag{49}$$

We now form the differences (48)$-$(49) and (48)$-(c_p T_g/h_{fg})$ (49) to give

$$\frac{DV_g}{V_g}\left(1 - \frac{V_g^2}{a_{e2}^2}\right) - \left(1 - \frac{c_p T_g}{h_{fg}}\right)\frac{\Delta T}{V_g \tau_T T_g} = 0, \tag{50}$$

$$\frac{DV_g}{V_g}\left(1 - \frac{V_g^2}{a_{e3}^2}\right) + \left(1 - \frac{c_p T_g}{h_{fg}}\right)\frac{D(\Delta T)}{T_g} = 0, \tag{51}$$

where a_{e2} and a_{e3} are defined by (41) and (42) respectively.

Equations (50) and (51) allow several important conclusions to be drawn concerning the flow behaviour in Type I waves:

(*a*) In a compressive wave, the pressure rises ($Dp > 0$), the velocity falls ($DV_g < 0$) and droplet evaporation occurs ($Dm_i < 0$). Equation (31) then shows that $\Delta T < 0$ and the vapour is superheated throughout the wave. From (50), for $DV_g < 0$ and $\Delta T < 0$, we deduce that $V_g < a_{e2}$. We have thus verified the statement that fully dispersed waves of Type I are only possible for $V_{g0} < a_{e20}$ and therefore the reference velocity a_{e2} takes on the role of a frozen speed of sound for such a wave.

(*b*) From (51) (noting that $DV_g < 0$ throughout) then, for $V_g > a_{e3}$, $D(\Delta T) < 0$ (superheat increases), and, for $V_g < a_{e3}$, $D(\Delta T) > 0$ (superheat decreases). The maximum superheat therefore occurs at that position in the wave where $V_g = a_{e3}$. We shall denote this velocity by a_{e3*}.

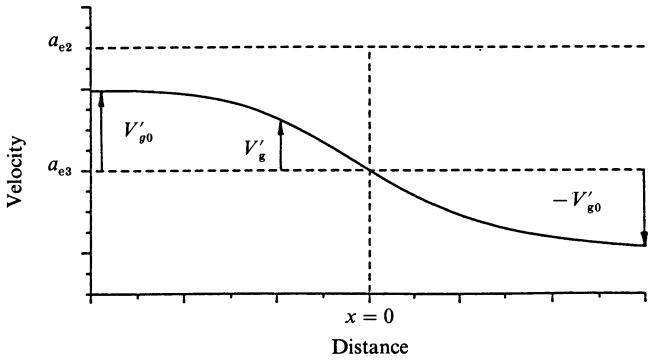

FIGURE 4. Schematic diagram of velocity distribution in a Type I wave to illustrate the notation.

We now define two Mach numbers (both based on the vapour phase velocity) by $M_{e2} = V_g/a_{e2}$ and $M_{e3} = V_g/a_{e3}$. Eliminating DV_g/V_g between (50) and (51) gives

$$\frac{D(\Delta T)}{T_g} + \frac{1-M_{e3}^2}{1-M_{e2}^2}\frac{\Delta T}{V_g \tau_T T_g} = 0. \tag{52}$$

From (52), we deduce the following:

(*a*) For $V_g < a_{e3}$ or $V_g > a_{e2}$, then $\Delta T > 0$ implies $D(\Delta T) < 0$ and $\Delta T < 0$ implies $D(\Delta T) > 0$. Hence, if the flow is disturbed from its equilibrium state, there is a tendency for it to return to that same equilibrium state. The behaviour in these regimes is therefore stable.

(*b*) For $a_{e3} < V_g < a_{e2}$, then $\Delta T > 0$ implies $D(\Delta T) > 0$ and $\Delta T < 0$ implies $D(\Delta T) < 0$. Small departures from thermal equilibrium have a tendency to grow and the behaviour is essentially unstable. It is this characteristic which is responsible for the existence of fully dispersed shock waves.

Equations (50) and (51) can now be solved simultaneously to obtain the velocity distribution in a Type I wave. To do this, we take as a reference condition the velocity a_{e3*} and define a perturbation velocity V'_g (see figure 4) by

$$V_g = a_{e3*} + V'_g. \tag{53}$$

All fully dispersed waves are weak and hence $(V'_g/a_{e3*}) \ll 1$. Substituting in (51) and retaining second-order terms (to model the nonlinear behaviour characteristic of all shock waves),

$$\frac{2V'_g}{a_{e3}^2}\frac{dV'_g}{dx} = \left(1 - \frac{c_p T_g}{h_{fg}}\right)\frac{1}{T_g}\frac{d(\Delta T)}{dx}. \tag{54}$$

In deriving (54), we have neglected the variation of a_{e3} through the wave and therefore dispense with the subscript *. (This minor assumption and others that follow are best justified *a posteriori* or by comparison with numerical solutions.)

Equation (54) can be approximately integrated subject to the boundary condition that far upstream of the wave $\Delta T \to 0$ and $V'_g \to V'_{g0}$. (V'_{g0} is the prescribed upstream velocity perturbation, see figure 4.) Thus,

$$\frac{V'^2_g - V'^2_{g0}}{a_{e3}^2} = \left(1 - \frac{c_p T_g}{h_{fg}}\right)\frac{\Delta T}{T_g}, \tag{55}$$

where it is understood that the coefficient of ΔT is a suitable average value. (In fact $c_p T_g/h_{fg}$ and RT_s/h_{fg} both vary only slightly through the wave and will be assumed constant in what follows.)

Equation (55) is a relationship between the non-equilibrium variable ΔT and the flow velocity. Far downstream of the wave, equilibrium is re-established ($\Delta T = 0$) and $V'_g = -V'_{g0}$. This is in keeping with Prandtl's relation $(a_{e3*}+V'_{g0})\ (a_{e3*}-V'_{g0}) = a^2_{e3*}$, providing squares of small quantities are neglected.

Substituting (55) into (50), we obtain

$$\tau_T \frac{dV'_g}{dx}\left[1-\left(\frac{a_{e3}}{a_{e2}}\right)^2\left(1+\frac{V'_g}{a_{e3}}\right)^2\right] = \frac{V'^2_g - V'^2_{g0}}{a^2_{e3}}. \tag{56}$$

We now introduce a dimensionless distance x_T, a dimensionless velocity perturbation v_T and a dimensionless parameter ϕ_T defined by

$$x_T = \left(\frac{a_{e2}}{a_{e3}}\right)^2 \frac{x}{a_{e3}\tau_T}, \tag{57}$$

$$v_T = \frac{V'_g}{V'_{g0}}, \tag{58}$$

$$\phi_T = \frac{(a_{e2}/a_{e3})^2-1}{2(V'_{g0}/a_{e3})} = \frac{(a_{e2}/a_{e3})^2-1}{2(M_{e30}-1)}, \tag{59}$$

where M_{e30} represents the upstream Mach number based on a_{e3}. It is important to note that ϕ_T is completely independent of the droplet size distribution and depends only on M_{e30} and the ratio a_{e2}/a_{e3} (which is virtually constant through the wave). Values of ϕ_T range from 1 to ∞. $\phi_T \to \infty$ corresponds to $M_{e30} \to 1$, the limiting case of a very weak wave. $\phi_T = 1$ corresponds to $V_{g0} = a_{e20}$ ($M_{e20} = 1$), the upper limiting case for fully dispersed waves of Type I.

Using the definitions (57)–(59), equation (56) can be written in dimensionless form as

$$(\phi_T - v_T)\frac{dv_T}{dx_T} = \tfrac{1}{2}(v_T^2 - 1). \tag{60}$$

Equation (60) is a differential equation for the dimensionless velocity distribution in the wave and can be integrated to give

$$x_T = \ln\left\{\frac{(1-v_T)^{(\phi_T-1)}}{(1+v_T)^{(\phi_T+1)}}\right\} + \text{const.} \tag{61}$$

Setting the arbitrary constant to zero locates the origin, $x_T = 0$, at $v_T = 0$, i.e. at $V_g = a_{e3*}$.

Given the complexity of the two-phase flow, (61), which shows that the dimensionless velocity profile of a Type I wave depends on only one parameter ϕ_T which is independent of droplet size, is indeed a remarkable result. In fact the droplet size distribution only enters the equation in the scaling of the wave in the x-direction, x_T being linear in the reciprocal of thermal relaxation time.

Figure 5 shows the dimensionless velocity profiles for three values of ϕ_T. The curves themselves are universal, but the corresponding values of M_{e30} marked on the diagram for illustrative purposes refer to low-pressure steam flow at 0.5 bar and wetness fraction 0.1. It is interesting to note that the velocity profile is not

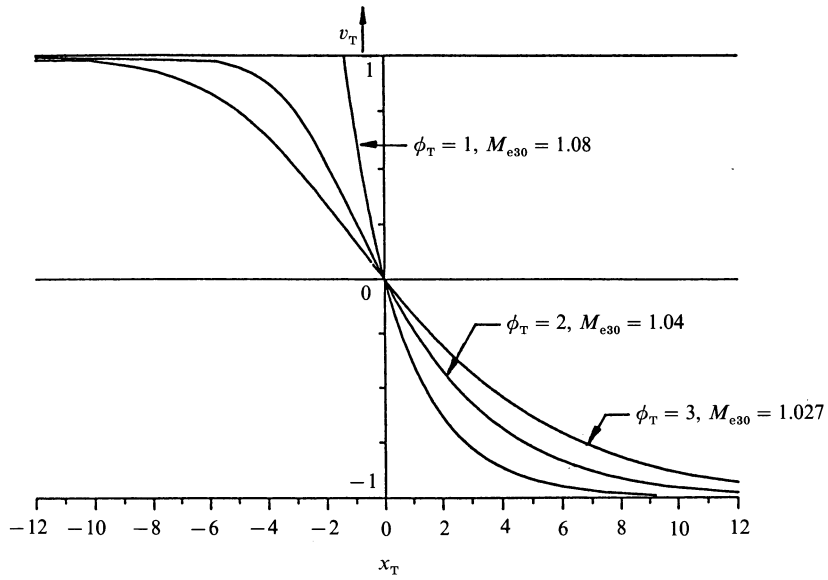

FIGURE 5. Dimensionless velocity profiles in a Type I wave.

symmetrical about $x_T = 0$ and that, for the upper limiting case $\phi_T = 1$, a discontinuity in the first derivative occurs at the leading tip of the wave ($v_T = 1$). This latter point will figure in the discussion of Type II waves, where it will also emerge that values of $\phi_T < 1$ in (61) have a physical significance.

A measure of the shock wave thickness is obtained by constructing the tangent to the velocity profile at $v_T = 0$ as shown in figure 6(*a*). From (60), $(\mathrm{d}v_T/\mathrm{d}x_T)_* = -\frac{1}{2}\phi_T$ and hence the dimensionless shock wave thickness $\Delta x_T = 4\phi_T$. The dimensional thickness is therefore given by

$$\Delta x = \frac{2a_{e3}\tau_T[1-(a_{e3}/a_{e2})^2]}{M_{e30}-1}. \tag{62}$$

In order to provide a physical appreciation of typical shock wave thicknesses, figure 6(*b*) presents curves of Δx versus droplet radius for different upstream Mach numbers M_{e30} for water droplets in steam at 0.5 bar pressure and 0.1 wetness fraction.

7.2. *Variation of the thermodynamic properties*

Knowing the velocity distribution, the pressure variation can be found from the momentum equation (4). Thus,

$$\frac{1}{p}\frac{\mathrm{d}p}{\mathrm{d}x} = \frac{-\gamma(a_{e3}+V'_g)}{(1-y)a_f^2}\frac{\mathrm{d}V'_g}{\mathrm{d}x}. \tag{63}$$

For fully dispersed waves, $V'_g \ll a_{e3}$, and integration subject to this and other obvious assumptions gives

$$\frac{p-p_*}{p_*} \approx \frac{-\gamma a_{e3}^2}{(1-y)a_f^2}(M_{e30}-1)\,v_T, \tag{64}$$

where p_* is the pressure at the reference state $V_g = a_{e3*}$. To a good approximation the pressure is a linear function of the dimensionless velocity perturbation v_T.

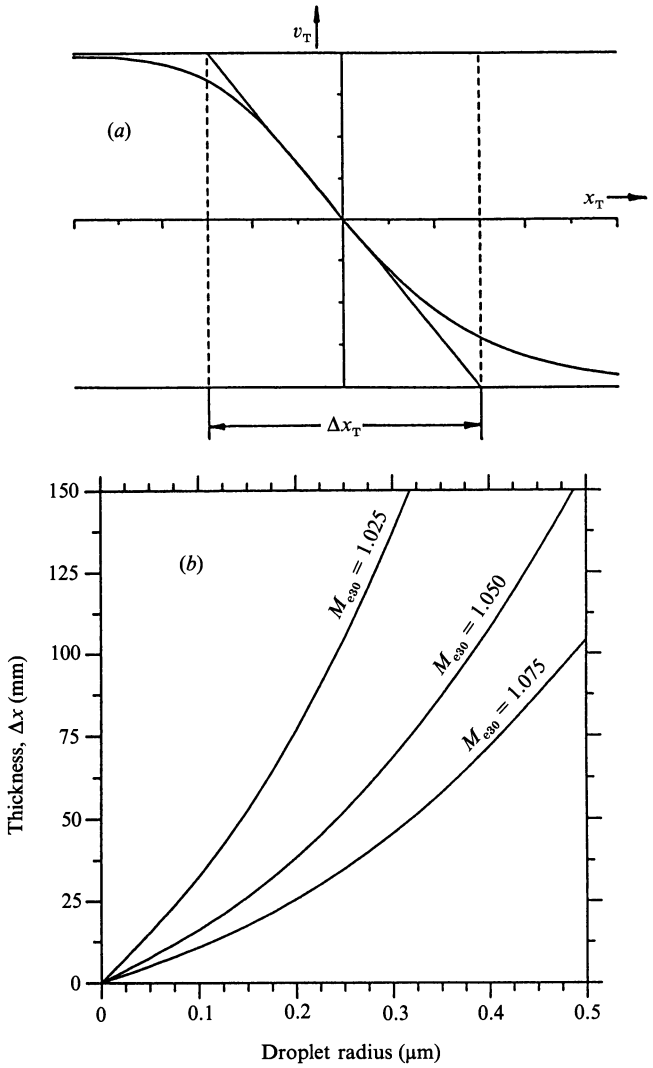

FIGURE 6. (*a*) Definition of shock wave thickness. (*b*) Thickness of Type I shock waves in wet steam; $p = 0.5$ bar, $y = 0.1$.

We showed earlier, in connection with (51), that the vapour superheat, $-\Delta T$, attains its maximum value when $V_g' = 0$. From (55), this maximum value is given by

$$\left(1-\frac{c_p T_g}{h_{fg}}\right)\frac{\Delta T_{max}}{T_g} = -(M_{e30}-1)^2. \tag{65}$$

We have thus arrived at the unexpected conclusion that the maximum superheat in a fully dispersed wave is independent of the droplet size distribution and (almost) the wetness fraction. The variation of ΔT through the wave can also be found from (55). Thus,

$$\left(1-\frac{c_p T_g}{h_{fg}}\right)\frac{\Delta T}{T_g} = -(M_{e30}-1)^2(1-v_T^2), \tag{66}$$

or, alternatively,

$$\frac{\Delta T}{\Delta T_{max}} = (1-v_T^2). \tag{67}$$

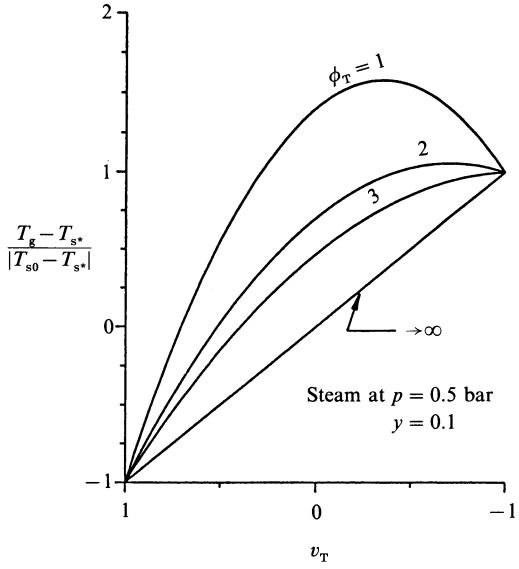

FIGURE 7. Vapour temperature distribution in a Type I wave as a function of velocity.

The departure from equilibrium in a fully dispersed wave can be surprisingly small. For example, for steam at 0.5 bar pressure and 0.1 wetness fraction, then for values of ϕ_T of 3, 2 and 1, $-\Delta T_{max}$ takes values of 0.5 °C, 1.1 °C and 4.2 °C respectively.

It is also interesting to calculate the vapour temperature distribution in the wave. The saturation temperature mimics the pressure distribution via the Clausius–Clapeyron equation and therefore increases monotonically through the wave,

$$\frac{T_s - T_{s*}}{T_{s*}} \approx \frac{RT_s}{h_{fg}} \frac{p - p_*}{p_*}, \tag{68}$$

where T_{s*} is the saturation temperature at pressure p_*. If T_{s0} is the upstream saturation temperature, then the increase in T_s through the wave is $2|T_{s0} - T_{s*}|$. We now define a dimensionless vapour phase temperature by

$$\frac{T_g - T_{s*}}{|T_{s0} - T_{s*}|} = \frac{T_g - T_s}{|T_{s0} - T_{s*}|} + \frac{T_s - T_{s*}}{|T_{s0} - T_{s*}|}. \tag{69}$$

Substituting from (64), (66) and (68), we obtain

$$\frac{T_g - T_{s*}}{|T_{s0} - T_{s*}|} = -v_T + \frac{(1-y)\, a_f^2 (M_{e30} - 1)}{\gamma a_{e3}^2 (RT_s/h_{fg})\,(1 - c_p T_g/h_{fg})} (1 - v_T^2). \tag{70}$$

Thus, for a given upstream Mach number and type of fluid, the vapour temperature distribution is a function only of v_T and is independent of the droplet size distribution. We see quite clearly now that the only way τ_T influences the wave profile for any of the thermodynamic properties is through the scaling in the x-direction. Thus, depending on the value of τ_T, the wave spreads out in the x-direction in such a way that, for each value v_T, the same values of p, ΔT and T_g result.

Figure 7 shows the vapour temperature distribution as a function of v_T for various values ϕ_T. These curves are not universal and do depend on the type of fluid and the upstream conditions as shown by (70). As before, we use as an illustrative example

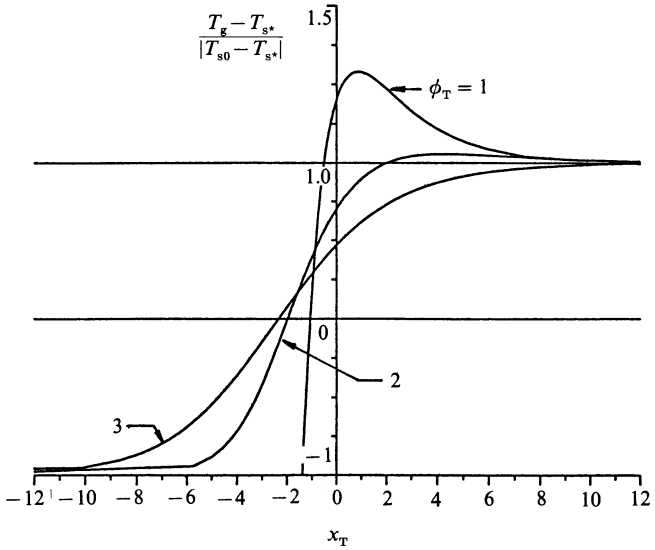

FIGURE 8. Vapour temperature distribution in a Type I wave as a function of distance, for steam at $p = 0.5$ bar, $y = 0.1$.

steam at 0.5 bar pressure and wetness fraction 0.1. The same curves plotted as functions of non-dimensionalized distance x_T are shown in figure 8. (It is interesting to compare the variation of thermodynamic and fluid properties through the wave (especially the temperature distribution) with similar calculations for other types of relaxing gas flows. In this respect the article by Becker & Bohme (1969) is particularly relevant.)

It is interesting to note that the vapour temperature rises above the downstream saturation temperature at some point in the wave if the far downstream velocity falls below a certain value. To see this, we solve (45)–(47) for $\mathrm{D}T_g/T_g$ to give

$$\frac{\mathrm{D}T_g}{T_g}\left(1-\frac{V_g^2}{a_{e2}^2}\right) = \left(1-\frac{V_g^2}{a_T^2}\right)\frac{\Delta T}{V_g \tau_T T_g}, \tag{71}$$

where

$$a_T^2 = \frac{(1-y)RT_g}{1+(RT_s/h_{fg})\,[y/(1-y)\,(c_f/R)\,(RT_s/h_{fg})-1]}. \tag{72}$$

Hence, for a superheated vapour $\Delta T < 0$, $\mathrm{D}T_g > 0$ for $a_T < V_g < a_{e2}$, and $\mathrm{D}T_g < 0$ for $V_g < a_T$. Evidently the velocity a_T plays the same role as the isothermal speed of sound in single-phase flow.

From the symmetry of the wave about $v_g = a_{e3*}$, we can estimate the upstream Mach number corresponding to a far downstream velocity of a_T. This is given by

$$M_{e30} = 1+(1-a_T/a_{e3}) = 2-a_T/a_{e3}. \tag{73}$$

For the sample calculation, vapour temperature overshoot should occur for $M_{e30} > 1.027$ and this agrees with the curves in figures 7 and 8.

7.3. *Comparison with numerical calculations*

In order to assess the accuracy of the analytical development presented in the previous sections, a computer program was written to integrate the equations of motion step-by-step through the wave. In the interests of accuracy, the basic

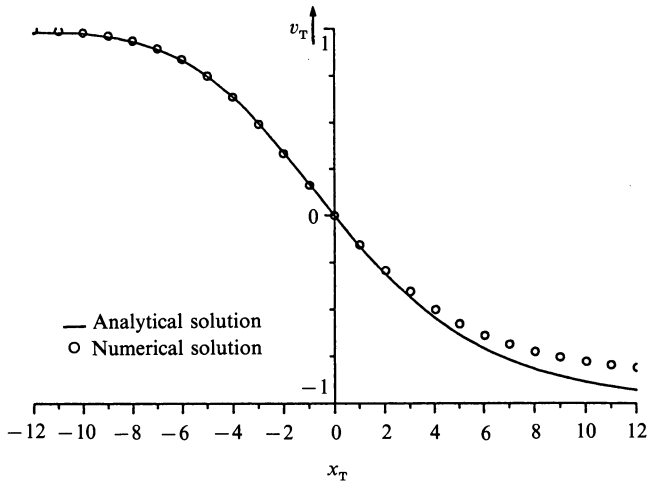

FIGURE 9. Velocity distribution in a Type I wave: comparison between theory and numerical calculation, $\phi_T = 3$.

equations (29)–(34) were employed in the code, the one simplification being that droplet temperature equilibration was assumed at all times. (For all the calculations presented here, droplet temperature relaxation was very fast, of the order of 0.01 μs.) Details of the numerical procedure can be found in Appendix B.

Figure 9 shows a comparison between the analytical and the numerical solutions for a typical type I wave. Not only does the analytical solution model the qualitative physical structure of the wave, but it also performs well on a quantitative basis.

7.4. *Velocity slip in Type I waves*

We are now in a position to assess the validity of our initial assumption of instantaneous velocity slip equilibration throughout Type I waves. The mathematical representation of this assumption is given by (44*b*). Non-dimensionalizing (by using (57)–(60)) and neglecting squares of small quantities, gives

$$\Delta v_i = -\left(\frac{a_{e2}}{a_{e3}}\right)^2 \frac{\tau_{Ii}}{\tau_T} \frac{1-v_T^2}{2(\phi_T - v_T)}, \tag{74}$$

where $\Delta v_i = \Delta V_i / V'_{g0}$ and ΔV_i is the i-group slip velocity.

Equation (74) gives the variation of velocity slip assuming instantaneous equilibration and neglecting any transient accommodation. A study of the velocity profiles in figure 5 suggests that the validity of this assumption might deteriorate as ϕ_T approached unity, especially near the wave tip ($v_T = 1$) where the velocity gradient is particularly high.

This possibility can be investigated by rederiving (51), but this time starting from (35)–(37) and including the slip velocity terms explicitly. Doing this, we obtain

$$\frac{DV_g}{V_g}\left(1-\frac{V_g^2}{a_{e3}^2}\right)+\left(1-\frac{c_p T_g}{h_{fg}}\right)\frac{D(\Delta T)}{T_g}+\frac{V_g^2}{a_{e3}^2}\sum y_i \frac{D(\Delta V_i)}{V_g} = 0. \tag{75}$$

Using the same integration technique as for (52) results in

$$\frac{V_g'^2 - V_{g0}'^2}{a_{e3}^2} - \left(1-\frac{c_p T_g}{h_{fg}}\right)\frac{\Delta T}{T_g} - \frac{V_g^2}{a_{e3}^2}\sum y_i \frac{\Delta V_i}{V_g} = 0. \tag{76}$$

A comparison of (55) and (76) shows that a necessary condition for the assumption of velocity slip equilibration to be valid is

$$\left|\sum y_i \frac{\Delta V_i}{V_g}\right| \ll \left|\left(1-\frac{c_p T_g}{h_{fg}}\right)\frac{\Delta T}{T_g}\right|. \tag{77}$$

Substituting from (59), (66) and (74), this condition can be rewritten, as

$$\frac{\phi_T}{\phi_T - v_T}\frac{1}{1-(a_{e3}/a_{e2})^2}\frac{y\tau_I}{\tau_T} \ll 1, \tag{78}$$

where $\tau_I = \sum y_i \tau_{Ii}/y$ is a weighted average of τ_{Ii}. For monodispersed droplets, $\tau_I/\tau_T = O(y)$ and typically we might expect $a_{e3}/a_{e2} \approx 0.95$. Thus, the condition (78) becomes

$$\frac{\phi_T y^2}{\phi_T - v_T} \ll 0.1. \tag{79}$$

As the analysis is restricted to low wetness fractions ($y < 0.2$), this inequality is well satisfied for most Type I waves. Remembering that $1 < \phi_T < \infty$ and $-1 < v_T < +1$, it can be seen that significant errors only occur as ϕ_T approaches unity and even then, only in the region close to $v_T = 1$.

We have therefore reached the important conclusion that departures from velocity slip equilibrium are only significant in Type I waves near the leading tip of the wave as the upstream Mach number approaches the upper limiting value $M_{e20} = 1$.

8. Fully dispersed waves of Type II

In analysing Type I waves, we assumed that droplet temperatures and velocity slip were at equilibrium and the transient time required to attain these conditions was negligibly small. Maintaining those constraints, we then showed that a fully dispersed wave could only exist for $M_{e20} < 1$, and for $M_{e20} > 1$ a discontinuity would appear in the flow as shown in figure 10.

We also showed that, as $M_{e20} \to 1$ from below, departures from velocity slip equilibrium becomes significant near the leading tip of the wave. In practice, when $M_{e20} > 1$, the discontinuity is smoothed out by the dominating effect of velocity slip and a stable, fully dispersed wave can occur. The front part of the wave is steep and is governed by velocity relaxation. The tail of the wave extends over a much longer distance and its structure is governed (just as in a Type I wave) by thermal relaxation. Connecting the two regions is a transition section where the effects of velocity slip and thermal relaxation are of comparable magnitude (see figure 10).

The mathematical analysis of Type II waves is much more difficult than that of Type I. However, the forward and rearward parts of the wave both respond to simple techniques if suitable approximations are made.

In the tail of the wave, velocity slip equilibration is assumed and the governing equations (45)–(47) are identical to those for a Type I wave. Non-dimensionalizing exactly as before gives the same differential equation (56) for the velocity distribution. On integration we obtain (61), the only difference being that now $\phi_T < 1$ because $M_{e20} > 1$.

Figure 11 shows a plot of (61) for an arbitrary value of $\phi_T = 0.69$. The lower branch of the curve tends to the correct downstream boundary condition ($V'_g \to -V'_{g0}$ as

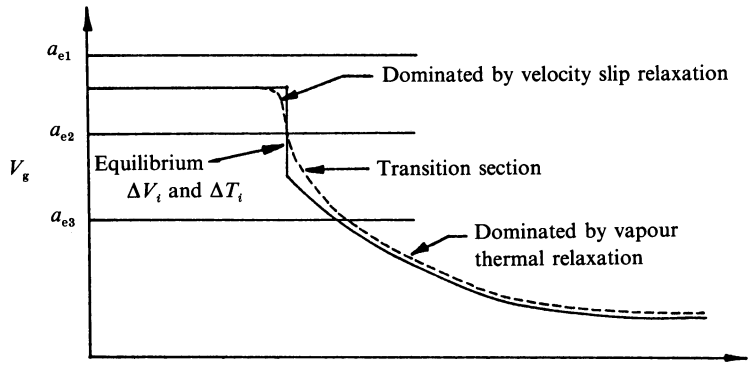

FIGURE 10. Schematic diagram of the velocity distribution in Type II waves.

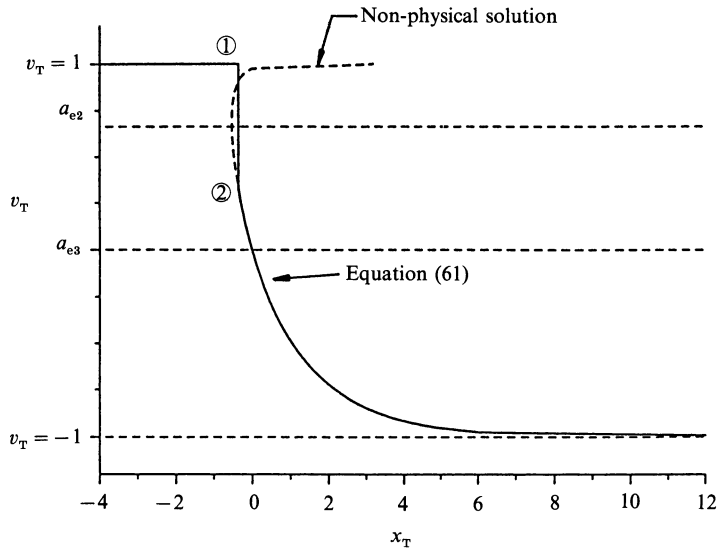

FIGURE 11. Structure of a Type II wave assuming equilibrium of droplet temperature and velocity throughout. $\phi_T = 0.69$, $M_{e20} = 1.036$.

$x \to \infty$), but the upper branch of the curve is obviously non-physical. Were we to continue to ignore the effects of velocity slip, we would replace the upper branch by the discontinuity shown in figure 10. Indeed, in many applications of condensing flows such an approximation would be quite acceptable. It is easy to locate the position of the discontinuity by using Prandtl's relation, $V_{g1} V_{g2} = a_{e2}^2$, subscripts 1 and 2 referring to the upstream and downstream conditions respectively as shown in figure 11.

We now investigate the process by which the effects of velocity slip smooth out the discontinuity at the front of the wave. In this very steep part of the velocity profile, we assume droplet temperature equilibration ($\tau_{Di} \to 0$, $\Delta T_i / \tau_{Di} \to V_i \mathrm{D}T_s$) and frozen heat transfer ($\tau_T \to \infty$). The former assumption is excellent, but the latter requires qualification. It is certainly not acceptable in the transition section of the wave but, unless the upstream Mach number M_{e20} is only just above unity, heat transfer plays only a minor role in modifying the velocity profile in the forward part of the wave.

Making these approximations results in a set of interphase transfer equations

represented by (29), (38) and (44a). Substituting in the conservation equations (35)–(37) then gives

$$\frac{\mathrm{D}p}{p}-\frac{\mathrm{D}T_\mathrm{g}}{T_\mathrm{g}}+\frac{\mathrm{D}V_\mathrm{g}}{V_\mathrm{g}}+\frac{y}{1-y}\frac{c_\mathrm{f}T_\mathrm{s}}{h_\mathrm{fg}}\frac{\mathrm{D}T_\mathrm{s}}{T_\mathrm{s}}=0, \tag{80}$$

$$\frac{\mathrm{D}p}{p}+\frac{V_\mathrm{g}^2}{RT_\mathrm{g}}\left\{\frac{\mathrm{D}V_\mathrm{g}}{V_\mathrm{g}}+\sum\frac{y_i}{1-y}\frac{\Delta V_i}{V_\mathrm{g}\tau_{\mathrm{I}i}V_\mathrm{g}}\right\}=0, \tag{81}$$

$$\frac{\mathrm{D}V_\mathrm{g}}{T_\mathrm{g}}+\frac{V_\mathrm{g}^2}{c_pT_\mathrm{g}}\left\{\frac{\mathrm{D}V_\mathrm{g}}{V_\mathrm{g}}+\sum\frac{y_i}{1-y}\frac{\Delta V_i}{V_\mathrm{g}\tau_{\mathrm{I}i}V_\mathrm{g}}\right\}=0. \tag{82}$$

Manipulating algebraically in much the same way as for Type I waves gives

$$\frac{\mathrm{D}V_\mathrm{g}}{V_\mathrm{g}}\left(1-\frac{V_\mathrm{g}^2}{a_{\mathrm{e}1}^2}\right)-\frac{V_\mathrm{g}^2}{a_{\mathrm{e}1}^2}\sum\frac{y_i}{1-y}\frac{\Delta V_i}{V_\mathrm{g}\tau_{\mathrm{I}i}V_\mathrm{g}}=0, \tag{83}$$

$$\frac{\mathrm{D}V_\mathrm{g}}{V_\mathrm{g}}\left(1-\frac{V_\mathrm{g}^2}{a_{\mathrm{e}2}^2}\right)+\frac{V_\mathrm{g}^2}{a_{\mathrm{e}1}^2}\sum\frac{y_i}{1-y}\frac{\mathrm{D}(\Delta V_i)}{V_\mathrm{g}}=0, \tag{84}$$

where $a_{\mathrm{e}1}$ is defined by (40).

Equations (83) and (84) bear a close resemblance to (50) and (51). For an initially equilibrium flow, the vapour lags the droplets as the flow decelerates through the wave and $\Delta V_i<0$ for all droplet groups. Equation (83) then shows that for $\mathrm{D}V_\mathrm{g}<0$ and $\Delta V_i<0$, it is necessary that $V_\mathrm{g}<a_{\mathrm{e}1}$ for a continuous solution to exist. The reference velocity $a_{\mathrm{e}1}$ therefore takes on the characteristic of a frozen speed of sound for Type II waves.

In considering (84), we note that the y_i are almost constant in the forward part of the wave (as negligible evaporation occurs here) and define an average slip velocity ΔV by

$$y\Delta V=\sum y_i\Delta V_i. \tag{85}$$

It then follows that when $V_\mathrm{g}>a_{\mathrm{e}2}$, $\mathrm{D}(\Delta V)<0$ and $|\Delta V|$ increases, and when $V_\mathrm{g}<a_{\mathrm{e}2}$, $\mathrm{D}(\Delta V)>0$ and $|\Delta V|$ decreases. The maximum value of $|\Delta V|$ therefore occurs at $V_\mathrm{g}=a_{\mathrm{e}2}$.

Eliminating $\mathrm{D}V_\mathrm{g}/V_\mathrm{g}$ from (83) and (84), we obtain

$$\frac{\mathrm{D}(\Delta V)}{V_\mathrm{g}}+\frac{1-M_{\mathrm{e}2}^2}{1-M_{\mathrm{e}1}^2}\sum\frac{y_i}{y}\frac{\Delta V_i}{V_\mathrm{g}\tau_{\mathrm{I}i}V_\mathrm{g}}=0, \tag{86}$$

where $M_{\mathrm{e}1}=V_\mathrm{g}/a_{\mathrm{e}1}$ is a vapour phase Mach number based on the sound speed $a_{\mathrm{e}1}$. Given that all the ΔV_i are negative, we deduce

(a) For $V_\mathrm{g}<a_{\mathrm{e}2}$ or $V_\mathrm{g}>a_{\mathrm{e}1}$, $\mathrm{D}(\Delta V)>0$ and $|\Delta V|$ decreases. The tendency for a flow disturbed from equilibrium is to return to the same equilibrium state.

(b) For $a_{\mathrm{e}2}<V_\mathrm{g}<a_{\mathrm{e}1}$, $\mathrm{D}(\Delta V)<0$ and $|\Delta V|$ increases. In this regime departures from equilibrium tend to grow and it is this characteristic which allows Type II fully dispersed waves to exist stably in steady flow.

Equation (86) can be integrated using the same technique as for Type I waves. This time, however, we take the velocity $a_{\mathrm{e}2*}$ as datum and define the vapour phase velocity perturbation V_g'' by,

$$V_\mathrm{g}=a_{\mathrm{e}2*}+V_\mathrm{g}''. \tag{87}$$

Approximate integration then gives

$$\frac{V_\mathrm{g}''^2-V_{g0}''^2}{a_{\mathrm{e}2}^2}=\frac{a_{\mathrm{e}2}^2}{a_{\mathrm{e}1}^2}\sum\frac{y_i\Delta V_i}{(1-y)\,a_{\mathrm{e}2}}, \tag{88}$$

where any variation of $a_{\mathrm{e}2}$ through the wave has been neglected.

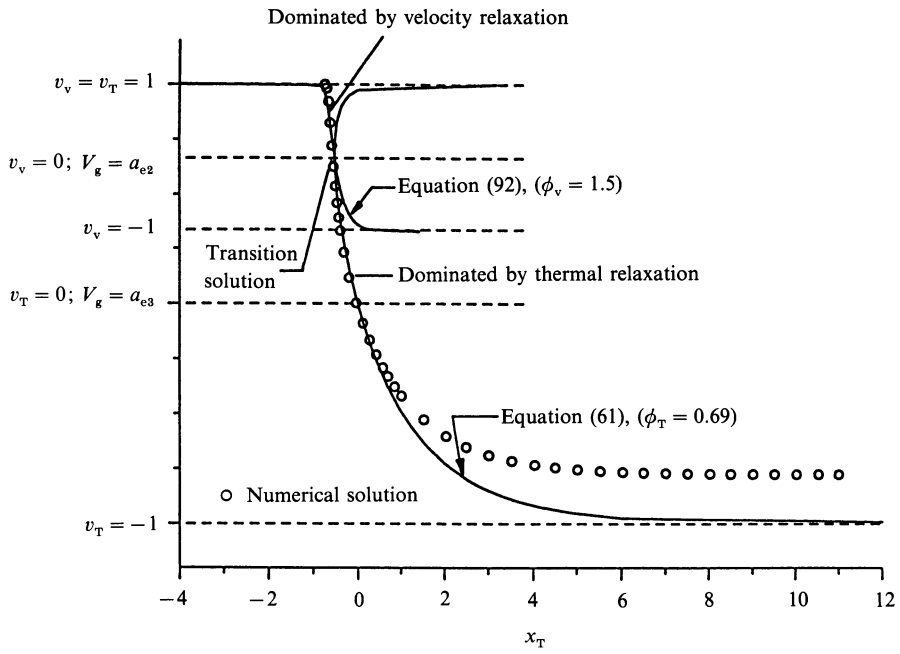

FIGURE 12. Velocity profile for a fully dispersed Type II wave.

It is difficult to proceed further with a general analysis involving a polydispersed droplet population as an average value of τ_{Ii} which is independent of the ΔV_i cannot be defined. (The problem did not arise with Type I waves because ΔT was common to all droplet groups). In order to make progress, therefore, we assume the droplet population to be monodispersed and introduce the following dimensionless variables:

$$x_v = \left(\frac{a_{e1}}{a_{e2}}\right)^2 \frac{x}{a_{e2}\tau_I}, \tag{89}$$

$$v_v = \frac{V_g''}{V_{g0}''}, \tag{90}$$

$$\phi_v = \frac{(a_{e1}/a_{e2})^2 - 1}{2(M_{e20} - 1)}. \tag{91}$$

The analysis parallels exactly that for Type I waves and leads to a solution for the velocity profile given by

$$x_v = \ln\left\{\frac{(1-v_v)^{(\phi_v-1)}}{(1+v_v)^{(\phi_v+1)}}\right\} + \text{const.} \tag{92}$$

Note that $\phi_v \to \infty$ corresponds to $V_{g0} \to a_{e2}$ ($M_{e20} \to 1$, the lower limit for a Type II wave) and $\phi_v = 1$ corresponds to $V_{g0} = a_{e1}$ ($M_{e10} = 1$, the upper limit for a Type II wave).

Figure 12 shows (61) and (92) plotted on the same scale for a value of $\phi_v = 1.5$ (which corresponds to the $\phi_T = 0.69$ of figure 11). The arbitrary constants in the equations have been adjusted empirically to show how the two solutions blend together in the transition section of the wave. Also shown in figure 12 are the results of a numerical integration for the same upstream conditions. The agreement between

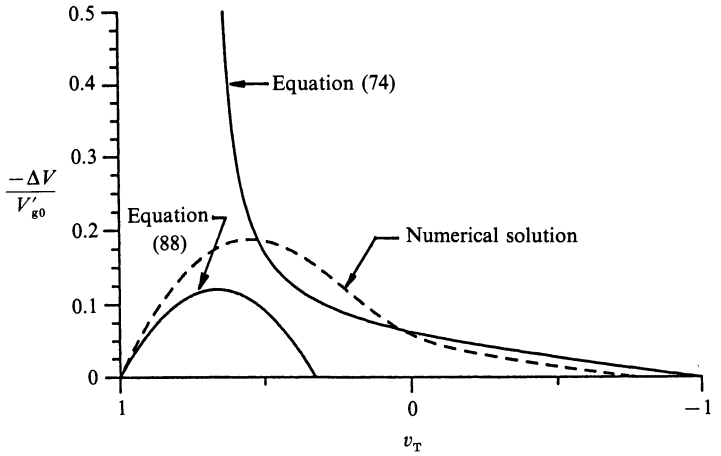

FIGURE 13. Velocity slip in a fully dispersed Type II wave.

the numerical and analytical solutions is generally good. The behaviour in the transition section of the wave is shown more clearly in figure 13 which is a graph of dimensionless velocity slip $\Delta V/V'_{g0}$ plotted as a function of v_T. In the forward part of the wave, the numerical solution is well approximated by (88) and in the rearward part it tends to (74) which assumes velocity slip equilibration.

9. Fully dispersed waves of Type III

When the upstream vapour velocity is in the range $a_{e10} < V_{g0} < a_{f0}$, a continuous solution of the equations of motion is impossible without relaxing the constraint on the droplet temperature. However, if this is done, a fully dispersed wave can exist, the leading tip of the wave being dominated by the effects of droplet temperature relaxation.

In practice, the difference between a_{e1} and a_f is always very small and so Type III waves are not of practical importance. In any case, the leading part of the wave is very steep indeed as the relaxation times τ_{Di} are very short, and under certain circumstances the thickness may even approach a value where the neglect of viscosity and thermal conductivity is not a good approximation.

Although it is possible to develop the equations of motion in a similar fashion as for the Type II wave analysis, we shall not do so here and be content to leave Type III waves as interesting curiosities of little practical significance.

10. The limiting case, $y \to 0$

In the analysis so far, we have assumed that the relative change in wetness fraction across a wave is comparatively small and that the relaxation times remain approximately constant. If the upstream wetness fraction y_0 is small, however, complete evaporation may occur in the wave and the flow behaviour changes.

Equations (40) and (41) show that, as $y \to 0$, both a_{e1} and a_{e2} tend to the frozen speed of sound a_f, but a_{e3} tends to a value given by (43) which is significantly below a_f. In this limiting case, the range of velocities available for Type II and Type III waves become negligibly small and it is only necessary to discuss the behaviour of Type I waves.

Consider first the velocity profile for the Type I wave labelled (*a*) in figure 14. This profile, which was computed numerically, corresponds to a monodispersed wet steam flow at a pressure of 0.5 bar, a wetness fraction of 0.1 and an arbitrary droplet radius of 0.1 μm. The changes in wetness fraction and thermal relaxation time across the wave are small and, in terms of the velocity change, the wave is almost centred on a_{e3}. Waves like this can be modelled very successfully by the analytical method developed in previous sections.

As y_0 tends to zero, all other parameters remaining constant, (24) shows that τ_T increases without limit. Under these circumstances it is not a good approximation to assume τ_T constant through the wave and it is necessary to resort to a computational method to obtain a quantitative solution to the equations of motion.

Curve (*b*) in figure 14 shows a case where $y_0 = 0.01$ and complete evaporation occurs in the wave. As $\tau_T \to \infty$, (50) and (52) show that both $DV_g \to 0$ and $D(\Delta T) \to 0$. Thus, when the droplets finally disappear, no further changes in velocity and temperature occur and, in fact, all the flow parameters remain constant at their local values. When this happens the far downstream velocity may well exceed the equilibrium sound speed a_{e3}, showing that a stationary wave can exist in a flow with both upstream and downstream velocities greater than a_{e3}. This is less surprising, however, when it is appreciated that the upstream flow is two-phase and is supersonic with respect to a_{e3}, while the downstream flow is single-phase and is subsonic with respect to a_f.

As y_0 is reduced further (curve *c* in figure 14), the wave gets progressively weaker and disappears altogether as $y_0 \to 0$. This type of flow behaviour and wave structure is reproduced for any upstream velocity in the range $a_{e30} < V_{g0} < a_{f0}$.

We are now in a position to deduce how the velocity of a small-amplitude plane wave propagating into a stationary vapour–droplet mixture varies as the wetness fraction of the mixture tends to zero. We assume that, however, it was generated, the compressional pulse has travelled a sufficient distance to have relaxed to its equilibrium velocity so that the flow is steady with respect to the wave.

Making the Type I wave approximations, we eliminate DV_g/V_g and DT_g/T_g from (35)–(37). Then, assuming y_0 is small, we integrate across the wave to give

$$\left(1-\frac{V_g^2}{a_f^2}\right)\frac{\Delta p}{p} \approx -\frac{\gamma V_g^2}{a_f^2}\left(\frac{h_{fg}}{c_p T_g}-1\right)\frac{\Delta y}{1-y}, \tag{93}$$

where Δp and Δy are the (small) changes in pressure and wetness fraction across the wave and V_g is the wave speed with respect to the stationary two-phase mixture.

Equation (93) is valid for all types of steady plane waves of small amplitude. In the limit when the flow is single phase, $\Delta y = 0$ and $V_g = a_f$ for all wave strengths $\Delta p/p$. When the flow is two-phase and in thermodynamic equilibrium on both sides of the wave the change in wetness fraction Δy_e is directly related to the pressure change Δp. This relationship, obtained simply from $\Delta h = \Delta p/\rho$ and the Clausius–Clapeyron equation, is given by

$$\left(1-\frac{c_p T_s}{h_{fg}}\right)\frac{\Delta p}{p} = -\frac{h_{fg}}{RT_s}\frac{\Delta y_e}{1-y}. \tag{94}$$

Combining (93) and (94) gives

$$\left(1-\frac{V_g^2}{a_{e3}^2}\right)\frac{\Delta p}{p} = 0, \tag{95}$$

with a_{e3} given by (43). Thus $V_g = a_{e3}$ for all values of $\Delta p/p$.

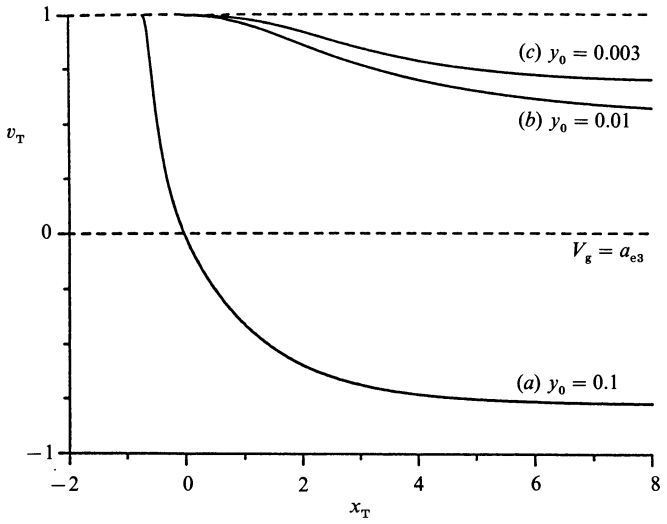

FIGURE 14. The behaviour of fully dispersed waves as $y_0 \to 0$. Steam of $p = 0.5$ bar, $r_0 = 0.1$ μm. (All solutions generated numerically.)

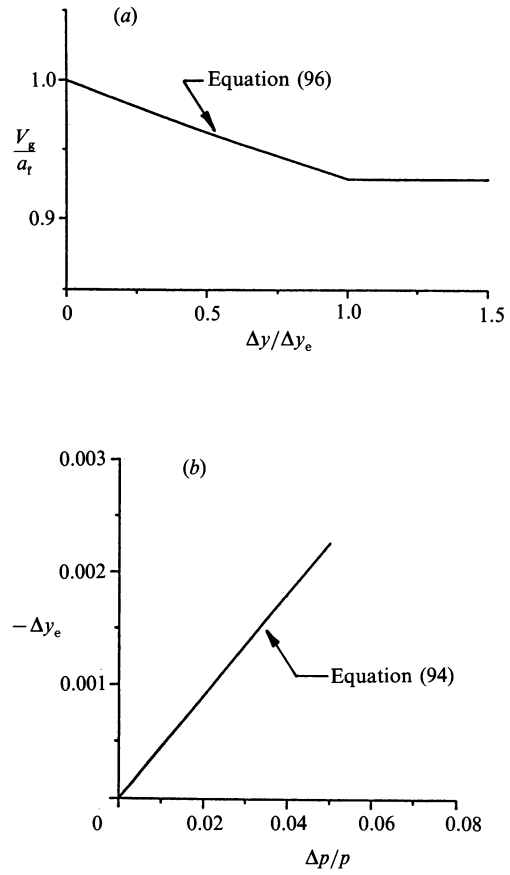

FIGURE 15. (*a*) Velocity of small-amplitude plane waves as $y_0 \to 0$. (*b*) Limiting wetness fraction for complete evaporation as a function of wave strength. Steam at 0.5 bar.

When complete evaporation occurs within the wave, Δp and Δy are independent variables (Δy is now equal to the upstream wetness fraction of the mixture) and (93) can then be solved for the wave speed V_g. For fixed wave strength $\Delta p/p$, V_g increases continuously from a_{e3} to a_f as $\Delta y \to 0$. This behaviour can be clearly seen by eliminating $\Delta p/p$ between (93) and (94) and solving for V_g to give,

$$V_g^2 = \frac{a_f^2}{[1+(\gamma-1)(1-c_p T_s/h_{fg})^2(\Delta y/\Delta y_e)]}, \tag{96}$$

which is valid for $0 \leqslant |\Delta y| \leqslant |\Delta y_e|$.

Figure 15 shows how the speed of an equilibrium small-amplitude wave in steam at a pressure of 0.5 bar varies as the wetness fraction tends to zero. Although the transition from a_{e3} to a_f is continuous, the wetness fraction is necessarily extremely small for all practical acoustic values of $\Delta p/p$ before any significant deviation from the equilibrium value a_{e3} is observed. Experimentally, the transition would appear discontinuous for all practical methods of measurement.

11. Partly dispersed shock waves

For $V_{g0} > a_{f0}$ no continuous solution of the conservation equations is possible and the dispersed part of the wave is preceded by a near discontinuity dominated by viscosity and thermal conductivity as shown in figure 3.

The usual model of a partly dispersed shock wave assumes that the interphase transfer processes are frozen during the passage through the discontinuity and the vapour properties just downstream of the discontinuity can be calculated using a standard Rankine–Hugoniot analysis. The liquid droplets therefore pass through the shock without change in radius, temperature and velocity. A comparison of the relaxation times τ_{Di}, τ_{Ii} and τ_{Ti} with the usual estimates of shock wave thickness (a few vapour mean free paths) shows this assumption to be quite acceptable, with the possible exception of droplet temperature relaxation.

The conditions downstream of the discontinuity provide the initial values for integrating the conservation equations through the relaxation zones. The droplet temperature relaxes very quickly, followed by velocity slip and finally the vapour temperature. The lengths of the relaxation zones are in the approximate ratios $\tau_D : \tau_I : \tau_T$. Marble (1969) deduced incorrectly that the velocity and thermal relaxation zones were of the same magnitude, but (26) show that $\tau_I/\tau_T = O(y)$.

For even moderate discontinuities, the values of $\Delta T_i/T_s$, $\Delta T/T_g$ and (especially) $\Delta V_i/V_g$ at the start of the relaxation zone are large and good accuracy can only be obtained if the calculations are performed numerically. As with other types of relaxing gas flow, a linearized solution for the relaxation zone is possible but this performs badly in comparison with the numerical calculations. When the shock is substantial, the magnitude of the aforementioned non-equilibrium variables is such that second-order effects involving $(\Delta V_i/V_g)^2$ etc. dominate the initial stage of relaxation and, when the shock is weak, the change of sign of the term $(1-M_{e3}^2)$ in (52) within the relaxation zone precludes the use of linearized theory.

The results of a typical numerical calculation for low-pressure steam are shown in figure 16. Upstream of the discontinuity, the flow is in equilibrium at a pressure of 0.5 bar and a wetness fraction of 0.1. The frozen Mach number M_{f0} is 1.5 and the droplets are monodispersed with radius 0.1 μm. The numerical results show that, downstream of the discontinuity, the droplet temperature relaxes very quickly as expected. The velocity slip, which is initially very large, then also relaxes and is

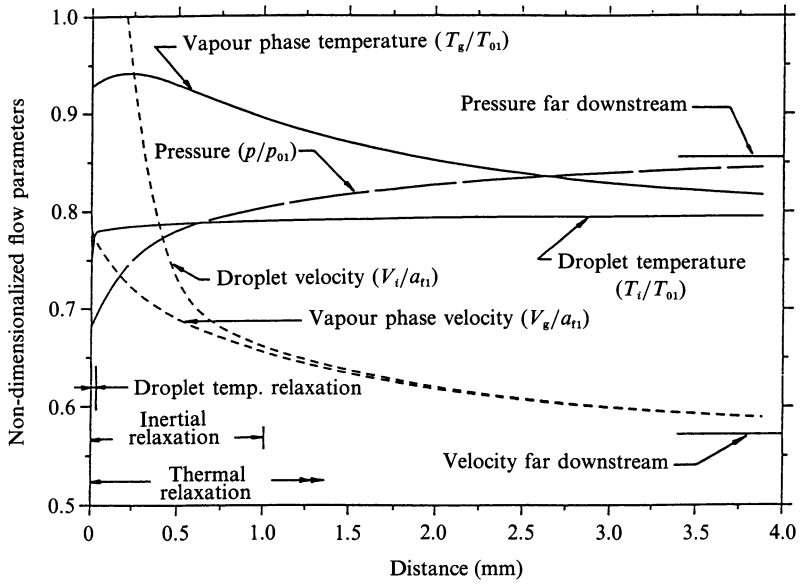

FIGURE 16. Structure of the relaxation zone for a typical partly dispersed shock wave in wet steam at upstream conditions $p = 0.35$ bar, $T = 345.9$ K, $r = 0.1$ μm, $y = 0.1$, $M_f = 1.5$.

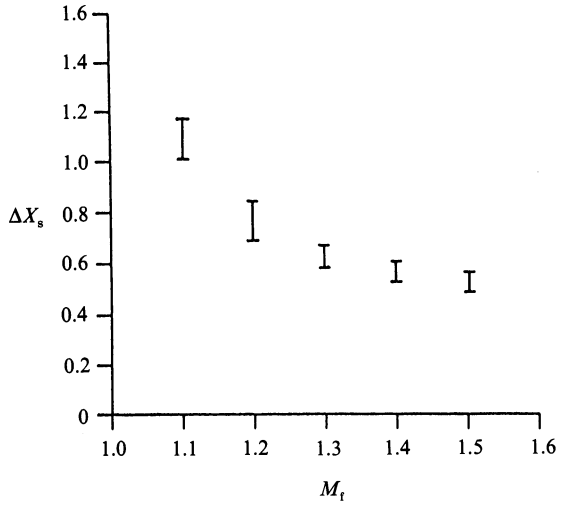

FIGURE 17. Dimensionless thickness of partly dispersed shock wave in wet steam. Steam at 0.5 bar, $r_0 = 0.1$–1.0 μm, $y_0 = 0.05$–0.1.

finally followed by the vapour superheat. The initial increase in vapour temperature just after the discontinuity is due to the effect of velocity slip.

A dimensionless shock wave thickness ΔX_s can be defined by

$$\Delta X_s = \frac{\int_0^\infty \Delta T \, \mathrm{d}x}{\Delta T_0 \tau_T V_{gd}}, \tag{97}$$

where ΔT_0 is the vapour superheat and V_{gd} is the velocity just downstream of the discontinuity. Figure 17 is a graph of ΔX_s as function of upstream Mach number M_f for a wide range of conditions for low-pressure steam–water droplet mixtures. Were

the superheat to decay exponentially in the relaxation zone as suggested by linearized theory, then ΔX_s would equal unity.

12. Conclusions

In this paper we have discussed the structure of stationary waves in steady, one-dimensional, vapour–droplet flows and have particularly concentrated on fully dispersed waves, which have not been addressed previously in the literature. The roles of the three relaxation processes in determining the structure of these waves have been clarified and an analytical method of solution has been presented, the results of which are comparable with those of accurate numerical calculations. The analysis predicts correctly the variation through the wave of the flow and thermodynamic properties, some of which, such as the vapour temperature, superheat and velocity slip, behave in initially surprising ways. The analysis also demonstrates the correct scaling parameters for such flows and clearly shows the effects in transonic flow situations of the common assumption of neglecting droplet temperature relaxation and velocity slip. The structure of partly dispersed shock waves, which is more straightforward, has also been briefly discussed and it has been noted that a linearized analysis for the relaxation zone does not, in general, give good results.

The derivation of the fundamental equations and much of the subsequent analytical development is valid for a polydispersed droplet population. In particular, we have described a method by which the effects of vapour thermal relaxation of an arbitrary liquid phase polydispersion may be elegantly incorporated into the analysis. Analytical difficulties still remain, however, if it is desired to include the effects of velocity slip with a wide range of droplet sizes present and such calculations are best performed numerically.

The wave behaviour in a two-phase flow as the wetness fraction tends to zero has been analysed and it has been shown that the notion of discontinuous behaviour at the saturation line, sometimes suggested in the literature, is fallacial. A continuous transition exists between the two limiting cases, a_{e3} and a_f.

This work was carried out at the Whittle Laboratory, University of Cambridge and A. Guha was supported by a Nehru Scholarship.

Appendix A. Thermal relaxation processes

Straightforward linearization of (17) in conjunction with (15), (18) and the Clausius–Clapeyron equation (9) results in

$$M_i \approx -4\pi r_i \frac{\mu}{4Kn_i}\frac{2q}{2-q}\left[\frac{h_{fg}}{RT_s}\frac{T_s-T_i}{T_s}+\frac{1-\alpha_i}{2}\frac{T_i-T_g}{T_s}\right], \tag{A 1}$$

where $\alpha_i = 1/(1+4.5Kn_i/Pr)$.

The steady-state value of the droplet temperature $T_{i\infty}$ is defined by setting the left-hand side of (12) to zero and introducing (16) and (A 1). The result is

$$T_{i\infty}-T_s = \frac{A}{1-A}(T_s-T_g), \tag{A 2}$$

where

$$A = (1-\alpha_i)\frac{RT_s}{h_{fg}}\left[\frac{1}{2}-\frac{4(2-q)}{9q}\frac{c_p T_s}{h_{fg}}\right]. \tag{A 3}$$

For most substances, irrespective of the Knudsen number and hence the value of α_i, the magnitude of $(T_{i\infty}-T_s)$ is a very small fraction of the vapour subcooling (T_s-T_g). (For example, for low-pressure steam with $q=1$ and $\alpha_i=0$, $A\approx 0.025$ and hence $|T_{i\infty}-T_s|<0.025\,|T_s-T_g|$.) Thus, the steady-state droplet temperature $T_{i\infty}$ is always approximately equal to the saturation temperature (the possible exception being if $q\ll 1$).

By substituting (16) and (A 1) in (12) and then eliminating $(T_{i\infty}-T_s)$ using equation (A 2), we obtain

$$\frac{dT_i}{dx}+\frac{T_i-T_{i\infty}}{V_i\tau_{Di}}=0, \tag{A 4}$$

where τ_{Di} is given by (22). Equation (A 4) is a relaxation equation in standard form for the i-group droplet temperature and τ_{Di} is the corresponding relaxation time.

In order to deduce an expression for the vapour thermal relaxation time, we imagine a departure from equilibrium solely of the vapour temperature T_g, the droplet temperatures remaining at the saturation value and the slip velocities being zero. Manipulation of the conservation equations (3)–(6) for the condition of zero velocity slip gives the thermodynamic relation

$$\frac{d}{dx}[(1-y)h_g+\Sigma y_i h_i]=\frac{1-y}{\rho_g}\frac{dp}{dx}. \tag{A 5}$$

Expansion of the left-hand side of (A 5) and introduction of (A 1), (11), (12) and (16) results in,

$$\frac{d(\Delta T)}{dx}+\frac{\Delta T}{V_g\tau_T}=\frac{RT_s}{h_{fg}}\left(1-\frac{h_{fg}}{c_pT_s}\right)\frac{T_s}{p}\frac{dp}{dx}, \tag{A 6}$$

where

$$\frac{1}{\tau_T}=\Sigma\frac{1}{\tau_{Ti}}, \tag{A 7}$$

τ_{Ti} being given by (24). $\Delta T=(T_s-T_g)$ is the vapour subcooling and is the non-equilibrium variable for this relaxation process and τ_T is the conjugate relaxation time. More details of the derivation of (A 6) and a discussion of the physical implications can be found in Young (1984).

Appendix B. Numerical solution procedure

Using (3), the conservation of droplet number, and (7) and (8), the equations of state for the vapour phase, the continuity, momentum and energy equations (4)–(6) may be recast as a set of three simultaneous equations for dV_g/dx, dT_g/dx and dp/dx. Equations (3) and (29)–(31) furnish expressions for dV_i/dx, dn_i/dx, dT_i/dx and dm_i/dx, a set of four such equations being obtained for each droplet group i. The resulting set of $(3+4N)$ simultaneous first-order differential equations (N being the number of droplet groups) can then be integrated numerically using a fourth-order Runge–Kutta procedure.

A computational procedure that marches forward in space must necessarily start from an initial condition that represents a deviation from equilibrium. For a partly dispersed shock wave, the difference in the vapour and liquid-phase flow variables just downstream of the frozen shock discontinuity constitute the required initial departure from equilibrium. For a fully dispersed shock wave an initial, arbitrary perturbation of the flow must be specified. Step-by-step integration of the conservation equations then automatically generates the wave profile. Providing the initial perturbation is sufficiently small, the numerical results closely approach the

exact solution. Thus, if two calculations are performed for the same upstream flow conditions but with different initial small perturbations, it is possible to superpose the results by a relative shift in the x-direction.

REFERENCES

BAKHTAR, F. & TOCHAI, M. 1980 An investigation of two-dimensional flows of nucleating and wet steam by the time-marching method. *Intl J. Heat Fluid Flow*, **2**, 5–18.

BAKHTAR, F. & YOUSIF, F. H. 1974 Behaviour of wet steam after disruption by a shock wave. *Symp. on Multi-Phase Flow Systems, University of Strathclyde, Paper* G3. Inst. Chem. Engrs.

BARSCHDORFF, D. 1970 Droplet formation, influence of shock waves and instationary flow patterns by condensation phenomena at supersonic speeds. *Proc. 3rd Intl Conf. on Rain Erosion and Associated Phenomena, R.A.E., Farnborough*, pp. 691–705.

BECKER, E. & BOHME, G. 1969 In *Nonequilibrium Flows*, vol. 1 (ed. P. P. Wegener), chap. 2.

COLE, J. E. & DOBBINS, R. A. 1970 Propagation of sound through atmospheric fog. *J. Atmos. Sci.* **27**, 426–434.

CUNNINGHAM, E. 1910 On the velocity of steady fall of spherical particles through fluid medium. *Proc. R. Soc. Lond.* A **83**, 357–365.

GOOSSENS, H. W. J., CLEIJNE, J. W., SMOLDERS, H. J. & DONGEN, M. E. H. VAN 1988 Shock wave induced evaporation of water droplets in a gas-droplet mixture. *Exp. Fluids* **6**, 561–568.

GUMEROV, N. A., IVANDAEV, A. I. & NIGMATULIN, R. I. 1988 Sound waves in monodisperse gas–particle or vapour–droplet mixtures. *J. Fluid Mech.* **193**, 53–74.

GYARMATHY, G. 1964 Bases for a theory for wet steam turbines. *Bull.* 6 Inst. for Thermal Turbomachines, Federal Technical University, Zurich.

GYARMATHY, G. 1976 In *Two-Phase Steam Flow in Turbines and Separators* (ed. M. J. Moore & C. H. Sieverding), chap. 3. Hemisphere.

JACKSON, R. & DAVIDSON, B. J. 1983 An equation set for non-equilibrium two-phase flow, and an analysis of some aspects of chocking, acoustic propagation, and losses in low pressure wet steam, *Intl J. Multiphase Flow* **9**, 491–510.

KONORSKI, A. 1971 Shock waves in wet steam flow. *PIMP (Trans. Inst. Fluid Flow Machinery, Polish Acad. Sci.)* **57**, 101–109.

LABUNTSOV, D. A. & KRYUKOV, A. D. 1979 Analysis of intensive evaporation and condensation. *Intl J. Heat Mass Transfer* **22**, 989–1002.

MARBLE, F. E. 1969 Some gas dynamic problems in the flow of condensing vapours, *Astronautica Acta* **14**, 585–614.

MOHEBAN, M. & YOUNG, J. B. 1985 A study of thermal nonequilibrium effects in low-pressure wet steam turbines using a blade-to-blade time-marching technique. *Intl J. Heat Fluid Flow* **6**, 269–278.

MOZURKEWICH, M. 1986 Aerosol growth and the condensation coefficient for water: A review. *Aerosol Sci. Technol.* **5**, 223–236.

PETR, V. 1973 Variation of sound velocity in wet steam. *Wet Steam 4, Conf., University of Warwick, April 1973*, pp. 17–20. Inst. Mech. Engrs.

PETR, V. 1979 Non-linear wave phenomena in wet steam. *Eighth Conf. on Steam Turbines of Large Output, Plsen*, pp. 248–265.

SCHNERR, G. 1989 2-D transonic flow with energy supply by homogeneous condensation: onset condition and 2-D structure of steady Laval Nozzle flow. *Exp. Fluids* **7**, 145–156.

SKILLINGS, S. A. 1989 Condensation phenomena in a turbine blade passage. *J. Fluid Mech.* **200**, 409–424.

VINCENTI, W. G. & KRUGER, C. H. 1965 *Introduction to Physical Gas dynamics*, Chap. 8. R. E. Kreiger.

YOUNG, J. B. 1982 The spontaneous condensation of steam in supersonic nozzles. *PhysicoChem. Hydrodyn.* **3**, 57–82.

YOUNG, J. B. 1984 Semi-analytical techniques for investigating thermal non-equilibrium effects in wet steam turbines. *Intl J. Heat Fluid Flow*, **5**, 81–91.